Adaptive scaling of the learning rate by second order automatic differentiation

Alban Gossard, Frédéric de Gournay

Adaptive scaling of the learning rate by second order automatic differentiation

Frédéric de Gournay[1,2] degourna@insa-toulouse.fr

Alban Gossard[1,3] alban.paul.gossard@gmail.com

[1] Institut de Mathématiques de Toulouse; UMR5219; Université de Toulouse; CNRS

[2] INSA, F-31077 Toulouse, France [3] UPS, F-31062 Toulouse Cedex 9, France

August 9, 2022

Abstract

In the context of the optimization of Deep Neural Networks, we propose to rescale the learning rate using a new technique of automatic differentiation. If $(1C, 1M)$ represents respectively the computational time and memory footprint of the gradient method, the new technique increase the overall cost to either $(1.5C, 2M)$ or $(2C, 1M)$. This rescaling has the appealing characteristic of having a natural interpretation, it allows the practitioner to choose between exploration of the parameter set and convergence of the algorithm. The rescaling is adaptive, it depends on the data and on the direction of descent. The rescaling is tested using the simple strategy of exponential decay, a method with comprehensive hyperparameters that requires no tuning. When compared to standard algorithm with optimized hyperparameters, this algorithm exhibit similar convergence rates and is also empirically shown to be more stable than standard method.

1 Introduction

The optimization of Deep Neural Networks (DNNs) has received tremendous attention over the past years. Training DNNs amounts to minimize the expectation of non-convex random functions in a high dimensional space $\mathbb{R}^d$. If $\mathcal{J} : \mathbb{R}^d \to \mathbb{R}$ denotes this expectation, the problem reads

$$\min_{\Theta \in \mathbb{R}^d} \mathcal{J}(\Theta), \tag{1}$$

with Θ the parameters. Optimization algorithms compute iteratively Θ_k, an approximation of a minimizer of (1) at iteration k, by the update rule

$$\Theta_{k+1} = \Theta_k - \tau_k \dot{\Theta}_k, \tag{2}$$

where τ_k is the learning-rate and $\dot{\Theta}_k$ is the update direction. The choice of $\dot{\Theta}_k$ encodes the type of algorithm used. This work focuses on the choice of the learning rate τ_k.

There is a trade-off in the choice of this learning rate. Indeed high values of τ_k allows *exploration* of the parameters space and slowly decaying step size ensures *convergence* in accordance to the famous Robbins-Monro algorithm [35]. This decaying condition may be met by defining the step as $\tau_k = \tau_0 k^{-\alpha}$ with τ_0 being the initial step size and $\frac{1}{2} < \alpha < 1$ a constant. The choice of the initial learning rate and its decay are left to practitioners and these hyperparameters have to be tuned manually in order to obtain the best rate of convergence. For instance, they can be optimized using a grid-search or by using more intricated strategies [39], but in all generality tuning the learning rate and its decay factor is difficult and time consuming. The main issue is that the learning rate has no natural scaling. The goal of this work is to propose an algorithm that, given a direction $\dot{\Theta}_k$ finds automatically a scaling of the learning rate. This rescaling has the following advantages:

- The scaling is adaptive, it depends on the data and of the choice of direction $\dot{\Theta}_k$.
- The scaling expresses the exploration vs. convergence trade-off. Multiplying the rescaled learning rate by $1/2$ enforces convergence whereas multiplying it by 1 allows for exploration of the space of parameters.

This rescaling comes at a cost and it has the following disadvantages:

- The computational costs and memory footprint of the algorithm goes from $(1C, 1M)$ to $(1.5C, 2M)$ or $(2C, 1M)$.
- The rescaling method is only available to algorithms that yield directions of descent, it excludes momentum method and notably Adam-flavored algorithm.
- Rescaling is theoritically limited to functions whose second order derivative exists and does not vanish. This non-vanishing condition can be compensated by L^2-regularization.

1.1 Foreword

First recall that second order methods for the minimization of a deterministic $\mathcal{C}^2$ function $\Theta \mapsto \mathcal{J}(\Theta)$ are based on the second order Taylor expansion at iteration k:

$$\mathcal{J}(\Theta_k - \tau_k \dot{\Theta}_k) \simeq \mathcal{J}(\Theta_k) - \tau_k \langle \dot{\Theta}_k, \nabla \mathcal{J}(\Theta_k) \rangle + \frac{\tau_k^2}{2} \langle \nabla^2 \mathcal{J}(\Theta_k) \dot{\Theta}_k, \dot{\Theta}_k \rangle. \tag{3}$$

If the Hessian of $\mathcal{J}$ is positive definite, the minimization of the left-hand side leads to the choice

$$\dot{\Theta}_k = P_k^{-1} \nabla \mathcal{J}(\Theta_k) \text{ with } P_k \simeq \nabla^2 \mathcal{J}(\Theta_k) \tag{4}$$

Once a direction $\dot{\Theta}_k$ is chosen, another minimization in τ_k entails

$$\tau_k = \frac{\langle \dot{\Theta}_k, \nabla \mathcal{J}(\Theta_k) \rangle}{\|\dot{\Theta}_k\|^2 c(\Theta_k, \dot{\Theta}_k)}, \tag{5}$$

where c is the curvature of the function, and is defined as

$$c(\Theta_k, \dot{\Theta}_k) \stackrel{\text{def}}{=} \frac{\langle \nabla^2 \mathcal{J}(\Theta_k) \dot{\Theta}_k, \dot{\Theta}_k \rangle}{\|\dot{\Theta}_k\|^2}. \tag{6}$$

A second-order driven algorithm can be decomposed in two steps: i) the choice of P_k in (4), and if this choice leads to an update which is a direction of ascent, that is $\langle \dot{\Theta}_k, \nabla \mathcal{J}(\Theta_k) \rangle > 0$, ii) a choice of τ_k by an heuristic inspired from (6) and (5).

In the stochastic setting, we denote as $s \mapsto \mathcal{J}_s$ the mapping of the random function. At iteration k, only information on $(\mathcal{J}_s)_{s \in \mathcal{B}_k}$ can be computed where $(\mathcal{B}_k)_k$ is a sequence of mini-batches which are indepently drawn. If $\mathbb{E}_{s \in \mathcal{B}_k}$ is the empirical average over the mini-batch, we define $\mathcal{J}_{\mathcal{B}_k} = \mathbb{E}_{s \in \mathcal{B}_k}[\mathcal{J}_s]$. Given Θ, the quantity $\mathcal{J}(\Theta)$ is deterministic, and $\mathcal{J}$ is the expectation of $\mathcal{J}_s$ w.r.t. s.

1.2 Related works

Choice of P_k: The choice $P_k = \nabla^2 \mathcal{J}_{\mathcal{B}_k}(\Theta_k)$ in (4), leads to a choice $\tau_k = 1$ and to the so-called Newton method. It is possible in theory to compute the Hessian by automatic differentiation if it is sparse [43], but to our knowledge it has not been implemented yet. In [27], the authors solve $\dot{\Theta}_k = (\nabla^2 \mathcal{J}_{\mathcal{B}_k}(\Theta_k))^{-1} \nabla \mathcal{J}_{\mathcal{B}_k}(\Theta_k)$ by a conjugate gradient which requires only matrix/vector product that is affordable by automatic differentiation [9, 30]. This point of view, as well as some variants [42, 20], suffer from high computational cost per batch and go through less data in a comparable amount of time, leading to slower convergence at the beginning of the optimization.

Another choice is to set $P_k \simeq \nabla^2 \mathcal{J}_{\mathcal{B}_k}(\Theta_k)$ in (4) which is coined as the "Quasi-Newton" approach. These methods directly invert a diagonal, block-diagonal or low rank approximation of the Hessian [5, 37, 36, 29, 28, 47]. In most of these works, the Hessian is approximated by $\mathbb{E}[\nabla \mathcal{J}_s(\theta_k) \nabla \mathcal{J}_s(\theta_k)^T]$, the so-called Fisher-Information matrix, which leads to the natural gradient method [3]. Note also the use of a low-rank approximation of the true Hessian for variance reduction in [14].

Finally, there is an interpretation of adaptive methods as Quasi-Newton methods. Amongst the adaptive method, let us cite RMSProp [41], Adam [19], Adagrad [13] Adadelta [48]. For all these methods P_k is as a diagonal preconditioner that reduces the variability of the step size accross the different layers. This class of methods can be written

$$\dot{\Theta}_k = P_k^{-1} m_k, \quad m_k \simeq \nabla \mathcal{J}(\Theta_k) \quad \text{and} \quad P_k \simeq \nabla^2 \mathcal{J}(\Theta_k). \tag{7}$$

For instance, RMSProp and Adagrad use $m_k = \nabla \mathcal{J}_{\mathcal{B}_k}(\Theta_k)$ whereas Adam maintains in m_k an exponential moving averaging from the past evaluations of the gradient. The RMSProp, Adam and Adagrad optimizers build P_k such that P_k^2 is a diagonal matrix whoses elements are exponential moving average of the square of the past gradients (see [34] for example) and is an estimator of the diagonal part of the Fisher-Information matrix.

All these methods can be incorporated in our framework as we consider the choice of P_k as a preconditioning technique whose step is yet to be found. In a nutshell, if P_k approximates the Hessian up to an unknown multiplicative factor, our method is able to find this multiplicative factor.

Barzilai-Borwein: The Barzilai-Borwein class of methods [4, 33, 11, 45, 6, 23] may be interpreted as methods which aim at estimating the curvature in (6) by numerical differences using past gradient computations. In the stochastic convex setting, the BB method is introduced in [40] for the choice $\dot{\Theta}_k = \nabla \mathcal{J}(\Theta_k)$ and also for variance-reducing [18] methods. It has been extended in [26] to non-convex problems and in [24] to DNNs. Due to the variance of the gradient and possibly to a poor estimation of the curvature by numerical differences, these methods allow to prescribe a new step at each epoch only. In [46, 8], the step is prescribed at each iteration at the cost of computing two mini-batch gradients per iteration. Moreover, in [46] the gradient over all the data needs to be computed at the beginning of each epoch whereas [8] maintains an exponential moving average to avoid this extra computation. The downside of [8] is that they still need to tune the learning rate and its decay factor and that their method has not been tried on other choices than $P_k = \mathrm{Id}$.

Our belief is that approximating by numerical differences in a stochastic setting suffers too much from variance from the data and from the approximation error, hence we advocate in this study exact computations of the curvature (6).

Automatic differentiation: The theory that allows to compute the matrix-vector product of the Hessian with a certain direction is well-studied [43, 9, 15, 30] and costs 4 passes (2 forward and backward passes) and 3 memory footprint, when the computation of the gradient costs 2 passes (1 forward and backward pass) and 1 memory footprint. We study the cost of computing the curvature defined in (6), which to the best of our knowledge, has never been studied. Our method has a numerical cost that is always lower than the best BB method [8].

1.3 Our contributions

We propose a change of point of view. While most of the methods presented above use first order information to develop second order algorithms, we use second order information to tune a first order method. The curvature (6) is computed using automatic differentiation in order to estimate the local Lipschitz constant of the gradient and to choose a step accordingly. Our contribution is threefold:

- We propose a method that automatically rescales the learning rate using curvature information (Section 2) and we discuss the heuristics of this method.
- We give the cost of computing the exact curvature (6) by automatic differentiation and compare it with numerical approximation (Section 3).
- The method is tested on a vanilla algorithm. The stability and advantages of the proposed algorithm are studied on different examples using the SGD and the RMSProp based optimizers (Section 4).

2 Rescaling the learning rate

A second order deterministic analysis such as the one in the beginning of Section 1 yields the following algorithm: given Θ_k and an update direction $\dot{\Theta}_k$, compute $c(\Theta_k, \dot{\Theta}_k)$ by (6), the step τ_k by (5) and finally update Θ_k by (2). The first order analysis requires the introduction of the local directional Lipschitz constant of the gradient

$$L_k = \max_{t \in [0, \tau_k]} |c(\Theta_k - t\dot{\Theta}_k, \dot{\Theta}_k)|, \tag{8}$$

that satisfies

$$\mathcal{J}(\Theta_k - \tau_k \dot{\Theta}_k) \leq \mathcal{J}(\Theta_k) - \tau_k \langle \dot{\Theta}_k, \nabla \mathcal{J}(\Theta_k) \rangle + \frac{\tau_k^2}{2} L_k \|\dot{\Theta}_k\|^2. \tag{9}$$

Introducing the rescaling

$$r_k = \langle \dot{\Theta}_k, \nabla \mathcal{J}(\Theta_k) \rangle / \left(\|\dot{\Theta}_k\|^2 L_k \right) \tag{10}$$

Then (9) turns into

$$\mathcal{J}(\Theta_k - \tau_k r_k \dot{\Theta}_k) \leq \mathcal{J}(\Theta_k) + \left(\tau_k^2 - \tau_k\right) \frac{L_k}{2} \|r_k \dot{\Theta}_k\|^2. \tag{11}$$

Any choice of τ_k in $]0, 1[$ leads to a decrease of (11). The choice of $\tau_k = \frac{1}{2}$ allows faster decrease of the right-hand side of (11). We coin the choice $\tau_k = 1$ in (11) as the "exploration choice" and the choice $\tau_k = \frac{1}{2}$ as the "convergence choice". The only difficulty in computing (10) is in computing L_k. Indeed, L_k is a maximum over an unknown interval and, in the stochastic setting, we only estimate the function $\mathcal{J}$ and its derivative on a batch $\mathcal{B}_k$. We propose to build $\tilde{L}_k$ an estimator of L_k, we replace the maximum by the value at $t = 0$ and we perform an exponential moving average in order to average over the previously seen data. A maximum of this exponential moving average with the current estimate is performed in order to stablize $\tilde{L}_k$. The algorithm reads as follows:

Algorithm 1 Rescaling of the learning rate

1: **Hyperparameters** $\varepsilon = 10^{-8}$ (numerical stabilization) and $\beta_3 = 0.9$ (exponential moving average).
2: **Initialization** $\hat{c}_0 = 0$
3: **Input (at each iteration k)**: a batch $\mathcal{B}_k$, $g_k = \mathbb{E}_{s \in \mathcal{B}_k}(\nabla \mathcal{J}_s(\Theta_k))$ and $\dot{\Theta}_k$ a direction that verifies $\langle g_k, \dot{\Theta}_k \rangle > 0$.
4: $c_k = \mathbb{E}_{s \in \mathcal{B}_k} \left[\left| \langle \nabla^2 \mathcal{J}_s(\Theta_k) \dot{\Theta}_k, \dot{\Theta}_k \rangle \right| \right] / \|\dot{\Theta}_k\|^2$ ▷ local curvature
5: $\hat{c}_k = \beta_3 \hat{c}_{k-1} + (1 - \beta_3) c_k \quad$ and $\quad \tilde{c}_k = \hat{c}_k / (1 - \beta_3^k)$ ▷ moving average
6: $\tilde{L}_k = \max(\tilde{c}_k, c_k)$ ▷ stabilization
7: $r_k = \langle \dot{\Theta}_k, g_k \rangle / \left(2 \|\dot{\Theta}_k\|^2 \tilde{L}_k \right)$ ▷ learning rate
8: **Output (at each iteration k)**: r_k, a rescaling of the direction $\dot{\Theta}_k$.
9: **Usage of rescaling**: The practitioner should use the update rule $\Theta_{k+1} = \Theta_k - \ell r_k \dot{\Theta}_k$, where $\ell = 1$ enforces exploration of the set of parameters and $\ell = \frac{1}{2}$ enforces convergence of the algorithm.

Note that curvature c_k is computed with the same batch that the one used to compute g_k and $\dot{\Theta}_k$. Several remarks are necessary to understand the limitations of rescaling.

Flatness of $\mathcal{J}$ and L_2 regularization (line 4) If the function $\mathcal{J}$ is locally affine in the direction $\dot{\Theta}$, then the curvature is zero and the rescaling r_k becomes infinite. A standard example is the Newton method of the 1D convex function $\mathcal{J}(\Theta) = \sqrt{1 + \Theta^2}$ which yields $\Theta_{k+1} = -\Theta_k^3$ and does not necessarily converge. This problem comes from the fact that the curvature $c(\Theta_k - t\dot{\Theta}_k, \dot{\Theta}_k)$ has to be computed for each $t \in [0, \tau_k]$ in order to estimate L_k in (8) but this quantity is only computed at $t = 0$. In DNN, the massive use of piecewise linear activation functions makes the Hessian vanish. Note that batch normalization [17] makes matters worse. Indeed suppose that batch normalization is used after a linear layer without bias. Let d_i be the matrix equal to 0 except for its line number i which is equal to the one of Θ. Denote E the vector space spanned by $(d_i)_i$. Choose a direction $\dot{\Theta} = \sum_i \lambda_i d_i$ in E. If the parameters are changed into $\Theta + t\dot{\Theta}$, then the i^{th} output neuron is multiplied by $(1 + t\lambda_i)$. This multiplication is cancelled by the batch-normalization if the latter is performed element-wise over the batch. The network is then insensitive to the directions in E. Since the gradient vanishes on E, theoritically it should not be seen by the method, but this vector space has huge dimension and numerical error can kick in and excite these directions. A similar effect can be seen when using convolutional layer, in this case the space E is the vector space spanned by each kernel. In order to partially solve this issue, we propose to use L_2 regularization, namely we add $\frac{\lambda}{2}\|\Theta\|^2$ to the loss function, this shifts the Hessian by $\lambda \mathrm{Id}$. In the area where the loss is convex, $\mathcal{J}$ becomes strictly convex and this improves the convergence even if it does not ensure it.

Gradient preconditioning In case of gradient preconditioning $\dot{\Theta}_k = P_k^{-1} g_k$ with $P_k \simeq \nabla^2 \mathcal{J}(\Theta_k)$, the advantage of rescaling is that the practitioner is allowed to approximate the Hessian up to a multiplicative factor. Suppose indeed that instead of providing a good estimate of the Hessian, the practitioner multiplies it at each iteration by an arbitrary factor $\alpha_k \in \mathbb{R}$. In this case, $\dot{\Theta}_k$ is multiplied by α_k^{-1} but the curvature c_k does not change. This means that $\hat{c}_k$ is independent of the previous $(\alpha_s)_{s \leq k}$. Finally, the rescaling r_k is multiplied by α_k. Hence the output of the algorithm $r_k \dot{\Theta}_k$ is independent of the sequence $(\alpha_s)_{s \leq k}$. Therefore, the practitioner does not need to worry about finding the right multiplicative factor, it is accounted for by the rescaling method.

Negativeness of the curvature (line 4) The main difference beween a first-order analysis (8) and a second-order (5) lies in handling the case when the curvature is negative. The first-order analysis, which we choose, relies on using absolute value of the curvature, when second-order analysis relies on more intricated methods, see [1, 7, 25, 10]. Note that the absolute value is taken inside the batch average in line 4 and not outside. Otherwise data in the batch where $\langle \nabla \mathcal{J}^2(\Theta_k)\dot{\Theta}_k, \dot{\Theta}_k \rangle$ is negative could compensate the data where it is positive, leading to a bad estimation of the curvature.

Estimating the Lipschitz constant (lines 4 to 6) The estimator of L_k must comply with two antagonist requirements. The first one is to average the curvature over the different batches to effectively compute the true curvature of $\mathcal{J}$. The second one is to use the local curvature at point Θ_k and in the direction $\dot{\Theta}_k$ which requires to forget old iterations. This advocates the use of an exponential moving average in line 5 with the parameter β_3. The maximum in Line 6 is reminiscent of the construction of AMSGrad [34] from Adam [19], it stabilize batches where $c_k \gg \tilde{c}_k$. In order to be consistent with the remark in ***Gradient preconditioning***, the averaged quantity is the one which does not depend on the unknown multiplicative factor α_k.

Convergence analysis We advertise that the choice $\ell = \frac{1}{2}$ enforces convergence. We make clear that it does not guarantee it. First, the analysis has been made in the non-stochastic setting. Second, in the non-stochastic setting, the proposed algorithm diverges for the 1D , striclty convex function $\Theta \mapsto \sqrt{1+\Theta^2}$. In order to recover the convergence results of [35], it is sufficient to sow instructions like

$$\alpha \leq \tau_k r_k k^\delta \leq \beta, \tag{12}$$

with fixed $\alpha, \beta > 0$ and $\delta \in]1/2, 1[$. This is the choice followed by [8] for instance. Note that convergence analysis for curvature-dependent step is, to our knowledge, studied only in [2], for the non-stochastic time-continuous setting.

3 Curvature computation

In this section, we state the result about the complexity of computing the curvature $c(\Theta, \dot{\Theta})$. Any DNN can be seen as a sequence of n operations (layers) that transforms the initial data x_0 into an output data x_n. This output x_n is then compared to a target via a loss function and we denote $x_{n+1} \in \mathbb{R}$ the result of this loss function. Each of the transformation may depend on some parameters θ_s, and they can be expressed as

$$x_{s+1} = \mathcal{F}_s(x_s, \theta_s), \quad \forall\, 0 \leq s \leq n. \tag{13}$$

In the above, $\mathcal{F}_s$ is the mapping of the s^{th} layer, x_n is the output, $\mathcal{F}_n$ is the loss function and $x_{n+1} \in \mathbb{R}$ is the value of the loss. Let $\Theta = (\theta_s)_{s=0..n}$ denote the set of parameters and $X = (x_s)_{s=0..n+1}$ the set of data as it is transformed through the neural network. The intermediate data x_s (resp. parameter θ_s) are supposed to belong to an Hilbert space $\mathcal{H}_s$ (resp. $\mathcal{G}_s$). For each s, we have $\mathcal{F}_s : \mathcal{H}_s \times \mathcal{G}_s \to \mathcal{H}_{s+1}$, and $\mathcal{H}_{n+1} = \mathbb{R}$.

The gradient of $\mathcal{J}$ with respect to Θ is computed using automatic differentiation. This requires to define the differentials of $\mathcal{F}_s$ with respect to its variables. Let $\partial_x \mathcal{F}_s : \mathcal{H}_s \to \mathcal{H}_{s+1}$, resp. $\partial_\theta \mathcal{F}_s : \mathcal{G}_s \to \mathcal{H}_{s+1}$, be the differential of $\mathcal{F}$ at the point (x_s, θ_s) w.r.t. x, resp. θ, and $(\partial_x \mathcal{F}_s)^\star$, resp. $(\partial_\theta \mathcal{F}_s)^\star$, its adjoint. Denote by $\nabla^2 \mathcal{F}_s$ the second order derivative tensor of $\mathcal{F}_s$ at the point (x_s, θ_s). The

backward of the data $\hat{X} = (\hat{x}_s)_{s=1..n+1}$ and the backward-gradient $\hat{\Theta} = (\hat{\Theta}_s)_{s=0..n}$ are defined by:

$$\begin{cases} \hat{x}_s = (\partial_x \mathcal{F}_s)^\star \hat{x}_{s+1} & \text{with } \hat{x}_{n+1} = 1 \\ \hat{\theta}_s = (\partial_\theta \mathcal{F}_s)^\star \hat{x}_{s+1}. \end{cases} \tag{14}$$

In Algorithm 2, the standard backpropagation algorithm is given as well as the modifications needed to compute the curvature.

Algorithm 2 Backpropagation with curvature computation

1: Compute and store the data $X = (x_s)_s$ with a forward pass (13).
2: Compute and store the backward $\hat{X} = (\hat{x}_s)_s$ and $\hat{\Theta} = (\hat{\theta}_s)_s$ using (14).
3: Then $\nabla \mathcal{J}(\Theta) = \hat{\Theta}$.
4: Choose any direction of update $\dot{\Theta} = (\dot{\theta}_s)_s$.
5: Compute the tangent $\dot{X} = (\dot{x}_s)_s$ with the following forward pass:

$$\dot{x}_{s+1} = (\partial_x \mathcal{F}_s)\dot{x}_s + (\partial_\theta \mathcal{F}_s)\dot{\theta}_s, \quad \dot{x}_0 = 0 \tag{15}$$

6: Then $\langle \nabla^2 \mathcal{J}(\Theta)\dot{\Theta}, \dot{\Theta} \rangle = \sum_s \langle \hat{x}_{s+1}, \nabla^2 \mathcal{F}_s(\dot{x}_s, \dot{\theta}_s) \otimes (\dot{x}_s, \dot{\theta}_s) \rangle_{\mathcal{H}_{s+1}}$.

The proof of this algorithm is postponed to the Appendix A. In the following theorem the complexity of computing this curvature is given.

Theorem 1 *If $(1C, 1M)$ represents respectively the computational time and memory footprint of the standard backpropagation method, Algorithm 2 costs either $(1.5C, 2M)$ or $(2C, 1M)$.*

By Algorithm 2, the computation of the curvature $c(\theta, \dot{\theta})$ requires 3 passes in total and the storage of X and $\hat{X}$ whereas the computation of the gradient requires 2 passes and the storage of X. Hence the memory footprint is multiplied by 2 and the computation time by 1.5. We show in Appendix A how to design a divide-and-conquer algorithm that changes this cost to $(2C, 1M)$. This result is of importance because it states that computing the exact curvature is at least as cheap as using numerical differences of the gradient [8].

4 Numerical experiments

The efficiency of the rescaling is tested in this section. We set ourselves in the case where the initial parameters are randomly chosen, so that the practitioner wants a smooth transition from exploring to converging. We choose in Algorithm 3 a simple, per epoch, exponential decay rule on the learning rate ℓ from 1 to 1/2. This algorithm is coined as RED (Rescaled with Exponential Decay). We purposely unplug any other tricks of the trade, notably Robbins-Monro convergence conditions. Indeed, a Robbins-Monro decay rule would interfere with our analysis. Algorithm RED is not a production algorithm, it serves at testing the "natural" properties of convergence of rescaling. In Appendix C.5, we provide a comparison of RED with a standard SGD that has Robbins-Monro decaying conditions. Due to the remark in Section 4, we make clear that L^2-regularization is used. If $\Theta \mapsto \mathcal{L}_s(\Theta)$ is the original loss function, then the function $\mathcal{J}_s$ is defined as $\mathcal{J}_s(\Theta) = \mathcal{L}_s(\Theta) + \frac{\lambda}{2}\|\Theta\|^2$.

The numerical experiments are done on the benchmark of [8]. It consists in four test cases, a MNIST classifier [22], a CIFAR-10 classifier [21] with VGG11 [38] architecture, a CIFAR-100 classifier with VGG19 and the classical autoencoder of MNIST described in [16]. The ReLU units are replaced by smooth versions in order to compute the curvature term, and L^2 regularization is added to each test. The models are trained with a batch size of 256 and the number of epochs is set to 200 for MNIST classification and 500 for the others. The precise set of parameters that allow reproductibility is described in the Appendix B. We also give indications of the computational time on an NVIDIA Quadro RTX 5000. Each experiment is run 3 times with different random seeds and we display the average of the tests with a bold line, the limits of the shadow area are given by the maximum and the minimum over the runs. When displaying the training loss or the step histories, an exponential moving average with a factor 0.99 is applied in order to smooth the curves and gain in visibility. To

Algorithm 3 RED (rescaled-exponential-decay) for SGD or RMSProp preconditioning **and no convergence guaranty**

1: **Input parameters** $\beta_2 = 0.999$ (RMSProp parameter), RMSProp (boolean), $\lambda > 0$ (L^2-regularization), N (total number of epochs), $\varepsilon = 10^{-8}$ (numerical stabilization).
2: **Initialization** $\hat{v}_0 = 0$, Θ_0 random, $\ell = 1$ initial step decay and $\eta = 1/2$ the step multiplicative factor between the first and the last iterations.
3: **for** $k = 1..$ **do**
4: $g_k = \mathbb{E}_{s\in\mathcal{B}_k}\left[\nabla \mathcal{J}_s(\Theta_k)\right]$ ▷ gradient
5: **if** RMSProp **then** ▷ RMSProp preconditioning
6: $\hat{v}_k = \beta_2 \hat{v}_{k-1} + (1-\beta_2) g_k^2$ and $\tilde{v}_k = \hat{v}_k/(1-\beta_2^k)$ and $P_k = \mathrm{diag}(\sqrt{\tilde{v}_k} + \varepsilon)$
7: **else** : $P_k = \mathrm{Id}$
8: **end if**
9: $\dot{\Theta}_k = P_k^{-1} g_k$ ▷ direction of update
10: **Use Algorithm 1 and compute** r_k ▷ rescaling
11: $\Theta_{k+1} = \Theta_k - \ell r_k \dot{\Theta}_k$ ▷ parameters update
12: At the end of each epoch $\ell \leftarrow \eta^{\frac{1}{N}} \ell$
13: **end for**

compare the stability of the algorithms, all the figures are duplicated in Appendix D where instead of displaying a moving average, the quantiles are shown per epoch for one of the three runs. Note that the training and testing loss functions are displayed with the L^2 regularization term. On all figures the x-axis is the number of epochs. Remember however that the computational cost is not the same for the different optimizers, see Theorem 1. In Appendix C, additional experiments are provided, where we push to the limit our algorithm, test it with momentum and compare it with [8].

4.1 RED vs manually-tuned learning rate

In this first set of experiments, we compare the RED method given in Algorithm 3 with standard SGD and RMSProp. In order to recover these two latter algorithms, set $r_k = 1$ in Line 10 of Algorithm 3. The hyperparameters, namely the initial learning rate ℓ and its decay factor η, are optimized on the training loss with a grid search over the 20% first epochs, these algorithm are coined as "standard algorithm". The results are displayed in Figure 1 for the standard algorithms (orange for SGD, blue for RMSProp) and their RED version (red for SGD, green for RMSProp).

Training loss The analysis of the training loss shows that RED is competitive to the standard SGD and RMSProp methods. Note however that the hyperparameters of the standard methods have been chosen as to optimize the behavior of the training loss, hence we cannot expect the RED method to outperform the manually-tuned methods. In Appendix C.3 we exhibit the scarce cases where RED is beaten by manually-tuned algorithms.

Step For CIFAR, we observe an increase in the steps at the beginning of the iterations which coincides to the important decrease of the training and testing loss functions. This might correspond to a search for a basin of attraction of a local minimum during roughly the first 50 epochs and then a convergence in this basin. It should be noted that the step of the standard CIFAR100 and autoencoder is an order of magnitude smaller than their RED counterpart. Indeed larger steps on these methods cause the algorithm to diverge. This seems to indicate that the stage of the first 10 epochs where the step is small is of importance and is well captured by the RED algorithm. The analysis of the step seems to showcase the power of adaptive rescaling.

Loss and test accuracy The rescaling aims at minimizing quickly the training loss, no conclusions can be drawn from the analysis of the test dataset. Nevertheless, on the CIFAR experiments, an overfitting phenomenon (minimum of the test loss) starts from the 25^{th} epoch approximatively. The overfitting is clearer and more pronounced on the RED method. This is in accordance with the analysis of the step size: the automatic method seems to have converged to the maximum of the expressivity of the network at the 50^{th} epoch. Concerning the accuracy, it is well known that adaptive

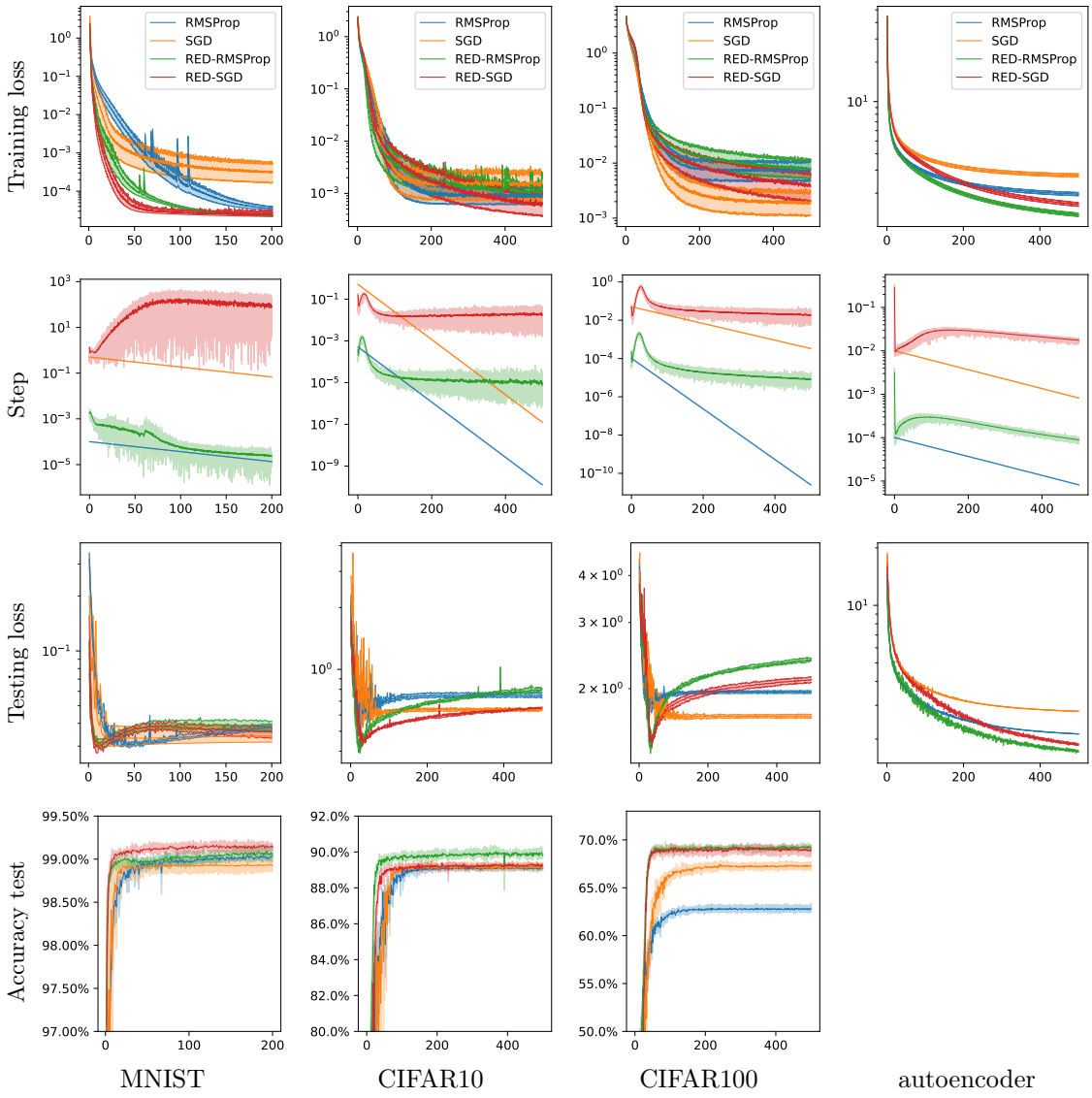

Figure 1: Training loss, step size, testing loss and test accuracy for the RED and manually-tuned SGD and RMSProp optimizers. Each column gives the different test cases (resp. MNIST, CIFAR10, CIFAR100 and autoencoder). The RED method which has no tuning gives competitive results in comparison with the manually-tuned SGD and RMSProp optimizers.

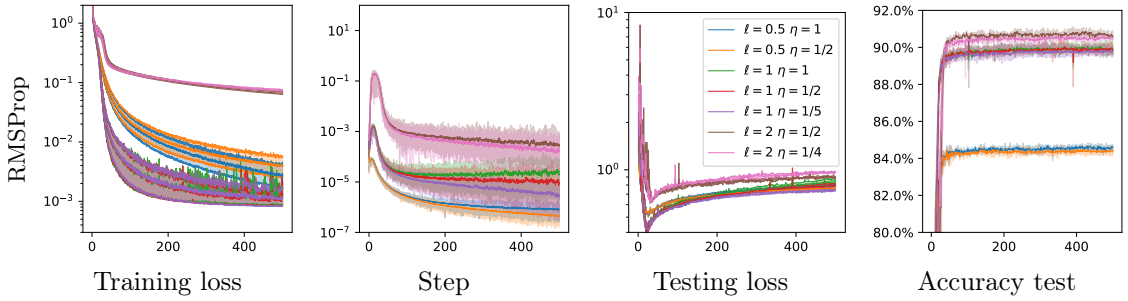

Figure 2: Training loss, step size, testing loss and test accuracy on the CIFAR10 classifier with auto-RMSProp. We use different values for the initial rescaled learning rate ℓ and its decay factor η. The basin of convergence mainly depends on the initial rescaled learning rate ℓ. The factor η stabilizes the method.

methods have poor generalization performances in the overparameterized setting in comparison to SGD [44]. Indeed the standard RMSProp achieves lower performance on the test dataset of CIFAR100. Surprisingly, the RED-RMSProp algorithm does not have this property.

As a conclusion of these tests, RED, which is a naive implementation of convergence/exploration trade-off works surprisingly well on this test-set. We purposely disconnected Robbins-Monro decay rule and the algorithm still exhibits convergence. However, the benchmark is simple and does not encompass every issue of modern machine learning. For example it allows for large batches, yielding good approximation of the gradient.

4.2 Influence of the step size and of the decay factor

The purpose of this section is to study influence of ℓ and η on the RED algorithm and to check the exploration/convergence interpretation. As a side gain, the results of this section are the kind of results a practitioner would obtain if he were to tune the hyperparameters ℓ and η of the RED algorithm on a validation set. We show-case that the validation results would be easily interpretable. The results are summarized in Figure 2 for the RMSProp optimizer on the CIFAR10 classifier.

It seems that the choice of ℓ determines the basin of attraction of the method, notice that the choice $\ell = \frac{1}{2}$ leads to a poor accuracy of the test, whereas the choice $\ell = 2$ leads to a poor training loss and testing loss. However, wether we are happy or not with a method depends on the criterion, the accuracy of the test for $\ell = 2$ is 1% higher. This is coherent with the belief that exploration matters at the beginning of the optimization process. The choice of ℓ determines the basin of attraction of the method. Concerning the choice of η, we spot instabilities in the training loss in the case $\ell = 1, \eta = 1$ from 200 to 500 epochs, these instabilities do not occur for the case $\eta = \frac{1}{5}$. This leads us to thinking that rescaling by $\frac{1}{2}$ indeed ensures convergence. Note that no instabilities are on the curves $\ell = \frac{1}{2}$ and some sort of instabilities (peaks in the testing loss and accuracy test) occur for the case $\ell = 2$. Extensive tests resulting in similar conclusions are reported in Appendix C.4.

4.3 Annealing

In order to showcase the accuracy of the rescaling, we propose a vanilla annealing method. We replace in Algorithm 3 (RED) the Line 12 (update of the parameter ℓ) by setting periodically $\ell = 1$ for 5 epochs, $\ell = \frac{1}{2}$ for 13 epochs and $\ell = 2$ for 2 epochs. These three phases are coined respectively as "exploration","convergence" and "hyper-exploration". We favor sharp changes when letting ℓ oscillate in order to easily interpret the results. This simple annealing method is coined RAn (Rescaled Annealing). We display in Figure 3 the results for CIFAR10 and CIFAR100. On Figure 3 the shift between the choice $\ell = \frac{1}{2}$ and $\ell = 2$ is represented by a vertical gray line. We also display the results for the RED algorithm for comparaison. Of importance in Figure 3 is the behavior of the loss function. The latter increases at each "hyper-exploration" phase, and converges during the exploration and convergence phase. A similar effect is also present but dimmer on the test loss and accuracy. It is difficult on this test to tell the difference between $\ell = 1$ and $\ell = \frac{1}{2}$, although it seems clear that $\ell = 2$ ensures an increase of the loss function, which is at the core of annealing method

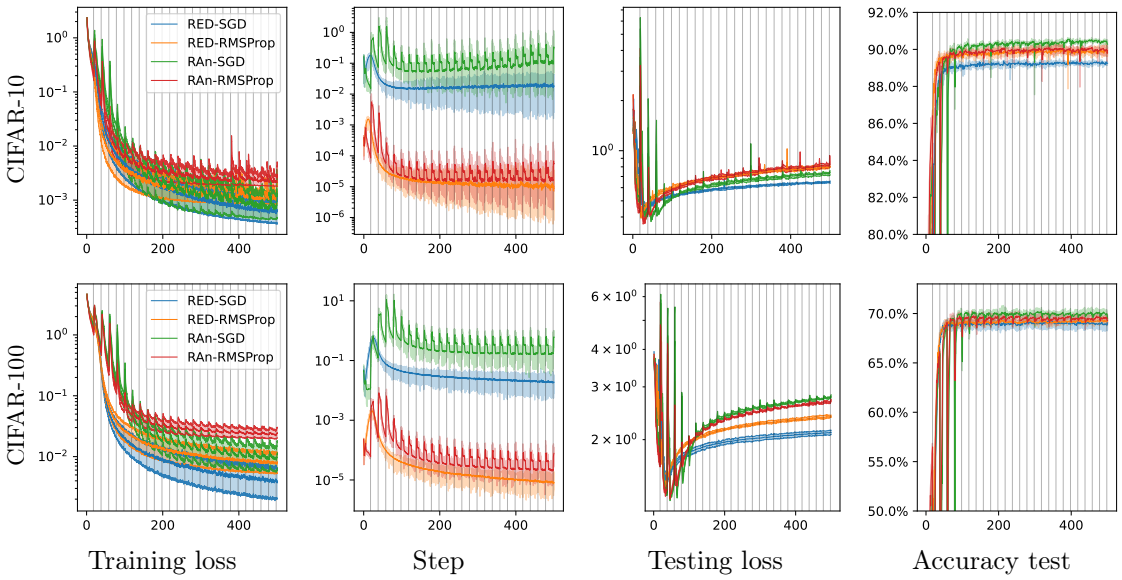

Figure 3: Annealing (RAn) vs Exponential decay (RED) method. The annealing method increases the loss functions during the hyperexploration ($\ell = 2$) phase (after the vertical gray lines). This empirically proves that the factor $\ell = 1$ is the limiting factor that allows exploration without increasing the loss function. The basis of attraction of the RAn method is different of the one of RED, except possibly for CIFAR10 with RMSProp.

that aim at escaping local minima. Considering accuracy of the test, it is clear that the RAn method finds a different local minima except maybe for the CIFAR10-RMSProp case.

4.4 Stability with respect to the averaging factor of the curvature

This section is dedicated to the study of the impact of the averaging factor of the curvature β_3 on the algorithm. A low value $\beta_3 \simeq 0$ yields an estimation of the curvature that is less dependent of the past iterations at the expense of having a higher variance. A value close to 1 results in a low variance estimation but that has a bias due to old iterations. In Figure 4, the CIFAR10 classifier is optimized using RED-SGD with values of $\beta_3 \in \{0, 0.5, 0.9, 0.99\}$. Interestingly, the parameter that gives the fastest increase of the test accuracy is $\beta_3 = 0$ at the cost of more instabilities. Although higher values of β_3 lead to an underestimation of the step size, the difference of performance on the training loss is insignificant. Overall, a value $\beta_3 \in [0.5, 0.99]$ has little impact on the convergence rate of the algorithm and a default value of $\beta_3 = 0.9$ can be considered. This parameter might be impacted by the batch size.

5 Conclusion and discussion

We developed a framework that allows automatic rescaling of the learning rate of a descent method via easily affordable second order information. This method introduces a new hyperparameter β_3 which has a physical meaning. The rescaled learning rate is data and direction adaptive, the practitioner have to choose between two scalings: 1/2 and 1 that solves the trade-off issue between exploration and stability. Numerical simulations show that a choice of exponential decrease is competitive to manual tuning of the step in the case of SGD and RMSProp preconditioning.

The main limitation of this method is that it does not provide a theoritical framework to deal with momentum since these methods do not necessarily yield directions of descent and do rely on per-iteration minimization of Lyapunov functions [31]. Another drawback is the need to use $\mathcal{C}^2$ activation functions, notably excluding ReLU. One way to circumvent this problem could be to work with smooth versions of the activation function in the training phase with an adaptive smoothing parameter. Finally, the curvature computation, also affordable in theory, requires additional implementations on top of ready-to-use machine learning librairies, which restricts our method to rather simple networks.

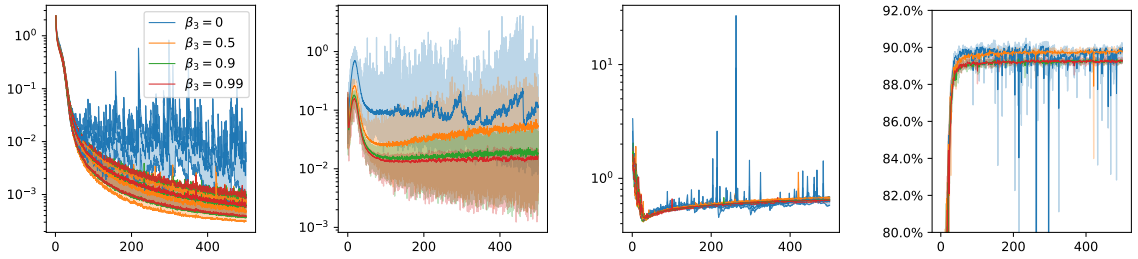

(a) Training loss (b) Step (c) Testing loss (d) Accuracy test

Figure 4: Training loss, step size, testing loss and test accuracy on the CIFAR10 classifier with auto-SGD. The tests are conducted with different values of the curvature averaging parameter β_3. A value $\beta_3 = 0$ yields instability and $\beta_3 \in [0.5, 0.99]$ has little impact on the convergence rate.

Numerical simulations hint that overfitting, when it happens, is more pronounced on the loss function for our method and that generalization of the RMSProp method is better.

References

[1] Zeyuan Allen-Zhu. Natasha 2: Faster non-convex optimization than sgd. *Advances in neural information processing systems*, 31, 2018.

[2] F Alvarez and A Cabot. Steepest descent with curvature dynamical system. *Journal of optimization theory and applications*, 120(2):247–273, 2004.

[3] Shun-Ichi Amari. Natural gradient works efficiently in learning. *Neural computation*, 10(2):251–276, 1998.

[4] Jonathan Barzilai and Jonathan M Borwein. Two-point step size gradient methods. *IMA journal of numerical analysis*, 8(1):141–148, 1988.

[5] Sue Becker and Yann Le Cun. Improving the convergence of back-propagation learning with second order methods. Technical Report CRG-TR-88-5, Department of Computer Science, University of Toronto, 1988.

[6] Fahimeh Biglari and Maghsud Solimanpur. Scaling on the spectral gradient method. *Journal of Optimization Theory and Applications*, 158(2):626–635, 2013.

[7] Yair Carmon, John C Duchi, Oliver Hinder, and Aaron Sidford. "convex until proven guilty": Dimension-free acceleration of gradient descent on non-convex functions. In *International Conference on Machine Learning*, pages 654–663. PMLR, 2017.

[8] Camille Castera, Jérôme Bolte, Cédric Févotte, and Edouard Pauwels. Second-order step-size tuning of sgd for non-convex optimization. *Neural Processing Letters*, pages 1–26, 2022.

[9] Bruce Christianson. Automatic hessians by reverse accumulation. *IMA Journal of Numerical Analysis*, 12(2):135–150, 1992.

[10] Frank E Curtis and Daniel P Robinson. Exploiting negative curvature in deterministic and stochastic optimization. *Mathematical Programming*, 176(1):69–94, 2019.

[11] Yuhong Dai, Jinyun Yuan, and Ya-Xiang Yuan. Modified two-point stepsize gradient methods for unconstrained optimization. *Computational Optimization and Applications*, 22(1):103–109, 2002.

[12] Alexandre Défossez, Léon Bottou, Francis Bach, and Nicolas Usunier. A simple convergence proof of adam and adagrad. *arXiv preprint arXiv:2003.02395*, 2020.

[13] John Duchi, Elad Hazan, and Yoram Singer. Adaptive subgradient methods for online learning and stochastic optimization. *Journal of machine learning research*, 12(7), 2011.

[14] Robert Gower, Nicolas Le Roux, and Francis Bach. Tracking the gradients using the hessian: A new look at variance reducing stochastic methods. In *International Conference on Artificial Intelligence and Statistics*, pages 707–715. PMLR, 2018.

[15] Andreas Griewank and Andrea Walther. *Evaluating derivatives: principles and techniques of algorithmic differentiation*. SIAM, 2008.

[16] Geoffrey E Hinton and Ruslan R Salakhutdinov. Reducing the dimensionality of data with neural networks. *science*, 313(5786):504–507, 2006.

[17] Sergey Ioffe and Christian Szegedy. Batch normalization: Accelerating deep network training by reducing internal covariate shift. In *International conference on machine learning*, pages 448–456. PMLR, 2015.

[18] Rie Johnson and Tong Zhang. Accelerating stochastic gradient descent using predictive variance reduction. *Advances in neural information processing systems*, 26, 2013.

[19] Diederik P Kingma and Jimmy Ba. Adam: A method for stochastic optimization. In *Proceedings of the International Conference on Learning Representations (ICLR)*, 2015.

[20] Shankar Krishnan, Ying Xiao, and Rif A Saurous. Neumann optimizer: A practical optimization algorithm for deep neural networks. In *Proceedings of the International Conference on Learning Representations (ICLR)*, 2018.

[21] Alex Krizhevsky, Geoffrey Hinton, et al. Learning multiple layers of features from tiny images. Technical report, Pennsylvania State University, 2009.

[22] Yann LeCun, Corinna Cortes, and CJ Burges. Mnist handwritten digit database. at&t labs, 2010.

[23] Ting Li and Zhong Wan. New adaptive barzilai–borwein step size and its application in solving large-scale optimization problems. *The ANZIAM Journal*, 61(1):76–98, 2019.

[24] Jinxiu Liang, Yong Xu, Chenglong Bao, Yuhui Quan, and Hui Ji. Barzilai–borwein-based adaptive learning rate for deep learning. *Pattern Recognition Letters*, 128:197–203, 2019.

[25] Mingrui Liu and Tianbao Yang. On noisy negative curvature descent: Competing with gradient descent for faster non-convex optimization. *arXiv preprint arXiv:1709.08571*, 2017.

[26] Ke Ma, Jinshan Zeng, Jiechao Xiong, Qianqian Xu, Xiaochun Cao, Wei Liu, and Yuan Yao. Stochastic non-convex ordinal embedding with stabilized barzilai-borwein step size. In *Proceedings of the AAAI Conference on Artificial Intelligence*, volume 32, 2018.

[27] James Martens et al. Deep learning via hessian-free optimization. In *International conference on machine learning (ICML)*, volume 27, pages 735–742, 2010.

[28] James Martens and Roger Grosse. Optimizing neural networks with kronecker-factored approximate curvature. In *International conference on machine learning*, pages 2408–2417. PMLR, 2015.

[29] Yann Ollivier. Riemannian metrics for neural networks i: feedforward networks. *Information and Inference: A Journal of the IMA*, 4(2):108–153, 2015.

[30] Barak A Pearlmutter. Fast exact multiplication by the hessian. *Neural computation*, 6(1):147–160, 1994.

[31] Boris Polyak and Pavel Shcherbakov. Lyapunov functions: An optimization theory perspective. *IFAC-PapersOnLine*, 50(1):7456–7461, 2017.

[32] Boris T Polyak. Some methods of speeding up the convergence of iteration methods. *Ussr computational mathematics and mathematical physics*, 4(5):1–17, 1964.

[33] Marcos Raydan. The barzilai and borwein gradient method for the large scale unconstrained minimization problem. *SIAM Journal on Optimization*, 7(1):26–33, 1997.

[34] Sashank J Reddi, Satyen Kale, and Sanjiv Kumar. On the convergence of adam and beyond. In *Proceedings of the International Conference on Learning Representations (ICLR)*, 2018.

[35] Herbert Robbins and Sutton Monro. A stochastic approximation method. *The annals of mathematical statistics*, pages 400–407, 1951.

[36] Nicolas Roux, Pierre-Antoine Manzagol, and Yoshua Bengio. Topmoumoute online natural gradient algorithm. *Advances in neural information processing systems*, 20, 2007.

[37] Tom Schaul, Sixin Zhang, and Yann LeCun. No more pesky learning rates. In *International conference on machine learning (ICML)*, pages 343–351. PMLR, 2013.

[38] Karen Simonyan and Andrew Zisserman. Very deep convolutional networks for large-scale image recognition. In *Proceedings of the International Conference on Learning Representations (ICLR)*, 2015.

[39] Samuel L Smith, Pieter-Jan Kindermans, Chris Ying, and Quoc V Le. Don't decay the learning rate, increase the batch size. *arXiv preprint arXiv:1711.00489*, 2017.

[40] Conghui Tan, Shiqian Ma, Yu-Hong Dai, and Yuqiu Qian. Barzilai-borwein step size for stochastic gradient descent. *Advances in neural information processing systems*, 29, 2016.

[41] Tijmen Tieleman and G Hinton. Divide the gradient by a running average of its recent magnitude. coursera neural netw. *Mach. Learn*, 6:26–31, 2012.

[42] Oriol Vinyals and Daniel Povey. Krylov subspace descent for deep learning. In *Artificial intelligence and statistics*, pages 1261–1268. PMLR, 2012.

[43] Andrea Walther. Computing sparse hessians with automatic differentiation. *ACM Transactions on Mathematical Software (TOMS)*, 34(1):1–15, 2008.

[44] Ashia C Wilson, Rebecca Roelofs, Mitchell Stern, Nati Srebro, and Benjamin Recht. The marginal value of adaptive gradient methods in machine learning. *Advances in neural information processing systems*, 30, 2017.

[45] Yunhai Xiao, Qiuyu Wang, and Dong Wang. Notes on the dai–yuan–yuan modified spectral gradient method. *Journal of computational and applied mathematics*, 234(10):2986–2992, 2010.

[46] Zhuang Yang, Cheng Wang, Zhemin Zhang, and Jonathan Li. Random barzilai–borwein step size for mini-batch algorithms. *Engineering Applications of Artificial Intelligence*, 72:124–135, 2018.

[47] Zhewei Yao, Amir Gholami, Sheng Shen, Mustafa Mustafa, Kurt Keutzer, and Michael W Mahoney. Adahessian: An adaptive second order optimizer for machine learning. In *Proceedings of the AAAI Conference on Artificial Intelligence*, 2021.

[48] Matthew D Zeiler. Adadelta: an adaptive learning rate method. *arXiv preprint arXiv:1212.5701*, 2012.

A Computation of the second order term

The goal of this section is to analyse the complexity of computing the curvature term and to prove Algorithm 2 and Theorem 1. We introduce a simple setting in order to retrieve the standard backpropagation algorithm. In Section A.2, we also give the expression of the matrix-vector product with the Hessian [9, 30], so that the link with other automatic-differentiation techniques can be made easily.

A.1 Proof of Algorithm 2

Forward pass A Neural Network $\mathcal{N}$ is a directed acyclic graph, at each node of the graph the data are transformed and fed to the rest of the graph. The data at the output x_n are then compared to y. Since there is no cycle in the graph, there is no mathematical restriction to turn such graph into a list. The set of parameters for layer s is denoted as θ_s, and we denote $\Theta = (\theta_s)_{s=0..n}$ the set of parameters of $\mathcal{N}$. The action of $\mathcal{N}$ is summed up in the following recurrence:

$$x_{s+1}(\Theta) = \mathcal{F}_s(x_s(\Theta), \theta_s), \quad 0 \leq s \leq n-1 \tag{16}$$

where $\mathcal{F}_s$ is the action of the s^{th} element (layer) of $\mathcal{N}$. We suppose that the comparison of x_n to y (the loss function) is encoded in the n^{th}-layer, so that $x_{n+1}(\Theta) = \mathcal{F}_n(x_n(\Theta), \theta_n)$ is a real number. We denote by $X(\Theta) = (x_s(\Theta))_{s=0..n}$ the set of data as it is transformed through $\mathcal{N}$. Each data $x_s(\Theta)$ is supposed to belong to an Hilbert space $\mathcal{H}_s$ and each parameter θ_s to an Hilbert space $\mathcal{G}_s$. We then have for each s

$$\mathcal{F}_s : \mathcal{H}_s \times \mathcal{G}_s \to \mathcal{H}_{s+1},$$

and $\mathcal{H}_{n+1} = \mathbb{R}$. Moreover the objective function $\mathcal{J}(\Theta)$ is exactly $x_{n+1}(\Theta)$. The computation of X through the recurrence (16) is denoted as the *forward pass*.

Tangent Given Θ, a set of data $X(\Theta)$, and an arbitrary direction $\dot{\Theta} = (\dot{\theta}_s)_{s=0..n}$, the tangent $\dot{X} = (\dot{x}_s)_{s=0..n}$ is defined as

$$\dot{x}_s = \lim_{\tau \to 0} \frac{x_s(\Theta + \tau\dot{\Theta}) - x_s(\Theta)}{\tau},$$

For each layer s, denote $\partial_x \mathcal{F}_s : \mathcal{H}_s \to \mathcal{H}_{s+1}$ (resp. $\partial_\theta \mathcal{F}_s : \mathcal{G}_s \to \mathcal{H}_{s+1}$) the differential of $\mathcal{F}_s$ with respect to the parameter x (resp. θ) at the point $(x_s(\Theta), \theta_s)$. We omit the notation of the point at which the differential is taken in order to simplify the notations. By the chain rule theorem, we have that if $\dot{x}_s$ exists, then the forward recurrence (16) yields

$$\dot{x}_{s+1} = (\partial_x \mathcal{F}_s)\dot{x}_s + (\partial_\theta \mathcal{F}_s)\dot{\theta}_s, \quad \dot{x}_0 = 0. \tag{17}$$

A recurrence on s allows to obtain existence of $\dot{X}$ and the scaling

$$X(\Theta + \tau\dot{\Theta}) = X(\Theta) + \tau\dot{X} + O(\tau^2).$$

Hence, if $X(\Theta)$ is computed and $\dot{\Theta}$ is chosen, then $\dot{X}$, the tangent in direction $\dot{\Theta}$ can be computed via the forward recurrence (17) and we have

$$\langle \nabla \mathcal{J}(\Theta), \dot{\Theta} \rangle = \dot{x}_{n+1}.$$

The recurrence (17) that allows the computation of $\dot{X}$ is coined as the *tangent pass*.

Adjoint/backward In order to compute the gradient, one resorts to the backpropagation algorithm which allows to reverse the recurrence (17) defining the tangent and to compute directly $\hat{\Theta} = (\hat{\theta}_s)_{s=0..n}$ such that

$$\langle \nabla \mathcal{J}(\Theta), \dot{\Theta} \rangle = \dot{x}_{n+1} = \sum_s \langle \dot{\theta}_s, \hat{\theta}_s \rangle_{\mathcal{G}_s}$$

The vector $\hat{\Theta}$ is then equal to $\nabla \mathcal{J}(\Theta)$, provided that one uses the scalar product induced by the sum of the scalar products in $\mathcal{G}_s$. To compute $\hat{\Theta}$, denote $\partial_x \mathcal{F}_s^\star : \mathcal{H}_{s+1} \to \mathcal{H}_s$ and $\partial_\theta \mathcal{F}_s^\star : \mathcal{H}_{s+1} \to \mathcal{G}_s$ the

adjoints of the differentials of $\mathcal{F}_s$. These adjoints are defined for all $\phi \in \mathcal{H}_{s+1}$ as the unique linear mapping that verifies:

$$\langle \partial_x \mathcal{F}_s^\star \phi, \psi \rangle_{\mathcal{H}_s} = \langle \phi, \partial_x \mathcal{F}_s \psi \rangle_{\mathcal{H}_{s+1}} \quad \forall \psi \in \mathcal{H}_s$$
$$\langle \partial_\theta \mathcal{F}_s^\star \phi, \psi \rangle_{\mathcal{G}_s} = \langle \phi, \partial_\theta \mathcal{F}_s \psi \rangle_{\mathcal{H}_{s+1}} \quad \forall \psi \in \mathcal{G}_s.$$

The backward of the data $\hat{X} = (\hat{x}_s)_{s=1..n+1}$ and the backward-gradient $\hat{\Theta} = (\hat{\Theta}_s)_{s=0..n}$ are defined by the reversed recurrence:

$$\begin{cases} \hat{x}_s = (\partial_x \mathcal{F}_s)^\star \hat{x}_{s+1} & \text{with } \hat{x}_{n+1} = 1 \\ \hat{\theta}_s = (\partial_\theta \mathcal{F}_s)^\star \hat{x}_{s+1}. \end{cases} \tag{18}$$

The definition of the adjoint and the formula of the tangent (17) give the following equality:

$$\begin{aligned} \langle \dot{x}_{s+1}, \hat{x}_{s+1} \rangle_{\mathcal{H}_{s+1}} &= \langle (\partial_x \mathcal{F}_s) \dot{x}_s + (\partial_\theta \mathcal{F}_s) \dot{\theta}_s, \hat{x}_{s+1} \rangle_{\mathcal{H}_{s+1}} \\ &= \langle \dot{x}_s, (\partial_x \mathcal{F}_s)^\star \hat{x}_{s+1} \rangle_{\mathcal{H}_{s+1}} + \langle \dot{\theta}_s, (\partial_\theta \mathcal{F}_s)^\star \hat{x}_{s+1} \rangle_{\mathcal{H}_{s+1}} \\ &= \langle \dot{x}_s, \hat{x}_s \rangle_{\mathcal{H}_s} + \langle \dot{\theta}_s, \hat{\theta}_s \rangle_{\mathcal{G}_s} \end{aligned} \tag{19}$$

Summing up the above equations for every s, we obtain:

$$\dot{x}_{n+1} = \langle \dot{x}_{n+1}, \hat{x}_{n+1} \rangle_{\mathcal{H}_{n+1}} = \langle \dot{x}_0, \hat{x}_0 \rangle_{\mathcal{H}_{n+1}} + \sum_s \langle \dot{\theta}_s, \hat{\theta}_s \rangle_{\mathcal{G}_s} = \sum_s \langle \dot{\theta}_s, \hat{\theta}_s \rangle_{\mathcal{G}_s},$$

where we used $\dot{x}_0 = 0$ and $\hat{x}_{n+1} = 1$. We then obtain the celebrated backward propagation formula:

$$\nabla \mathcal{J}(\Theta) = \hat{\Theta}.$$

The complexity analysis of the computation of the gradient by the backward formula shows that it requires the computation and the storage of the forward in order to be able to evaluate $(\partial_x \mathcal{F}_s)^\star$ and $(\partial_\theta \mathcal{F}_s)^\star$ at the point $(x_s(\Theta), \theta_s)$.

Computing the curvature Computing the gradient of $\mathcal{J}$ does not require to compute the tangent $\dot{X}$, because the recurrence (18) defining the backward $\hat{X}$ reverses the recurrence (17) that defines the tangent $\dot{X}$. This inversion is performed in (19). We show in this section that the tangent $\hat{X}$ also reverses the recurrence defining the second order term $\ddot{X}$ defined in (20) below. Once the direction $\dot{\Theta}$ is chosen, the curvature term can be computed by a forward pass. To this end, for any direction $\dot{\Theta}$, introduce $\ddot{X} = (\ddot{x}_s)_{s=0..n+1}$ by:

$$\ddot{x}_s = \lim_{\tau \to 0} \frac{x_s(\Theta + \tau \dot{\Theta}) - x_s(\Theta) - \tau \dot{x}_s}{\tau^2}, \tag{20}$$

where $\dot{x}_s$ is the tangent defined in (17). Denote also $\nabla^2 \mathcal{F}_s$ the bilinear symmetric mapping from $\mathcal{H}_s \times \mathcal{G}_s$ to $\mathcal{H}_{s+1}$ that represents the second order differentiation of $\mathcal{F}_s$ at point $(x_s(\Theta), \theta_s)$. It is defined as the only bilinear symmetric mapping that verifies for every (h_x, h_θ)

$$\begin{aligned} \mathcal{F}_s(x_s(\Theta) + h_x, \theta_s + h_\theta) =& \mathcal{F}_s(x_s(\Theta), \theta_s) + \partial_x \mathcal{F}_s h_x + \partial_\theta \mathcal{F}_s h_\theta + \frac{1}{2} \nabla^2 \mathcal{F}_s(h_x, h_\theta) \otimes (h_x, h_\theta) \\ &+ o(\|h_x\|^2 + \|h_\theta\|^2) \end{aligned}$$

It is easy to prove that $\ddot{x}_s$ exists and verifies:

$$\ddot{x}_{s+1} = (\partial_x \mathcal{F}_s) \ddot{x}_s + \frac{1}{2} \nabla^2 \mathcal{F}_s(\dot{x}_s, \dot{\theta}_s) \otimes (\dot{x}_s, \dot{\theta}_s), \quad \ddot{x}_0 = 0. \tag{21}$$

Indeed, denote $\xi_s = x_s(\Theta + \tau \dot{\Theta}) - x_s(\Theta) - \tau \dot{x}_s$ so that $\ddot{x}_s = \lim_{\tau \to 0} \frac{\xi_s}{\tau^2}$. We have

$$\begin{aligned} \xi_{s+1} &= \mathcal{F}_s(x_s(\Theta + \tau \dot{\Theta}), \theta_s + \tau \dot{\theta}_s) - \mathcal{F}_s(x_s(\Theta), \theta_s) - \tau (\partial_x \mathcal{F}_s) \dot{x}_s - \tau (\partial_\theta \mathcal{F}_s) \dot{\theta}_s \\ &= \mathcal{F}_s(\xi_s + x_s(\Theta) + \tau \dot{x}_s, \theta_s + \tau \dot{\theta}_s) - \mathcal{F}_s(x_s(\Theta), \theta_s) - \tau (\partial_x \mathcal{F}_s) \dot{x}_s - \tau (\partial_\theta \mathcal{F}_s) \dot{\theta}_s \\ &= (\partial_x \mathcal{F}_s) \xi_s + \frac{\tau^2}{2} \nabla^2 \mathcal{F}_s \left(\frac{\xi_s}{\tau} + \dot{x}_s, \dot{\theta}_s \right) \otimes \left(\frac{\xi_s}{\tau} + \dot{x}_s, \dot{\theta}_s \right) + o(\tau^2 + \|\xi_s\|^2). \end{aligned} \tag{22}$$

By a forward recurrence on (22), starting with $\xi_0 = 0$, we have that $\xi_s = O(\tau^2)$ so that $\ddot{x}_s$ exists. Dividing (22) by τ^2 and taking the limit yields (21).

Upon replacing $\dot{X}$ by $\ddot{X}$, the trick used in (19) can be applied and translates into:

$$\begin{aligned}\langle \ddot{x}_{s+1}, \hat{x}_{s+1}\rangle_{\mathcal{H}_{s+1}} &= \langle (\partial_x \mathcal{F}_s)\ddot{x}_s + \frac{1}{2}\nabla^2 \mathcal{F}_s(\dot{x}_s, \dot{\theta}_s)\otimes(\dot{x}_s,\dot{\theta}_s), \hat{x}_{s+1}\rangle_{\mathcal{H}_{s+1}} \\ &= \langle \ddot{x}_s, (\partial_x \mathcal{F}_s)^\star \hat{x}_{s+1}\rangle_{\mathcal{H}_{s+1}} + \frac{1}{2}\langle \nabla^2 \mathcal{F}_s(\dot{x}_s, \dot{\theta}_s)\otimes(\dot{x}_s,\dot{\theta}_s), \hat{x}_{s+1}\rangle_{\mathcal{H}_{s+1}} \\ &= \langle \ddot{x}_s, \hat{x}_s\rangle_{\mathcal{H}_s} + \frac{1}{2}\langle \nabla^2 \mathcal{F}_s(\dot{x}_s, \dot{\theta}_s)\otimes(\dot{x}_s,\dot{\theta}_s), \hat{x}_{s+1}\rangle_{\mathcal{H}_{s+1}}\end{aligned}$$

Summing up these equations in s and using $\ddot{x}_0 = 0$ and $\hat{x}_{n+1} = 1$, we obtain

$$\begin{aligned}\ddot{x}_{n+1} &= \langle \ddot{x}_{n+1}, \hat{x}_{n+1}\rangle_{\mathcal{H}_{n+1}} \\ &= \langle \ddot{x}_0, \hat{x}_0\rangle_{\mathcal{H}_{n+1}} + \sum_s \frac{1}{2}\langle \nabla^2 \mathcal{F}_s(\dot{x}_s, \dot{\theta}_s)\otimes(\dot{x}_s,\dot{\theta}_s), \hat{x}_{s+1}\rangle_{\mathcal{H}_{s+1}} \\ &= \sum_s \frac{1}{2}\langle \nabla^2 \mathcal{F}_s(\dot{x}_s, \dot{\theta}_s)\otimes(\dot{x}_s,\dot{\theta}_s), \hat{x}_{s+1}\rangle_{\mathcal{H}_{s+1}}\end{aligned}$$

In order to conclude and prove Algorithm 2, it is sufficient to remark that $\mathcal{J}(\Theta) = x_{n+1}(\Theta)$ so that $\frac{1}{2}\langle \nabla^2 \mathcal{J}(\Theta)\dot{\Theta}, \dot{\Theta}\rangle = \ddot{x}_{n+1}$. In order to settle the notations, we give some of the expression of $\nabla^2 \mathcal{F}_s(\dot{x}_s, \dot{\theta}_s)\otimes(\dot{x}_s,\dot{\theta}_s)$ for standard layers in Appendix A.4.

A.2 Hessian-vector dot product

We now turn our attention to showing how to compute $\nabla^2 \mathcal{J}(\Theta)\dot{\Theta}$ in our setting. The results are known [9, 30]. We emphasize that the computation of the curvature is simplier than the Hessian-vector product. In our setting, the trick that allows the computation of the Hessian-vector product is based on the following ideas

- The mapping $\dot{\Theta} \mapsto \frac{1}{2}\langle \nabla^2 \mathcal{J}(\Theta)\dot{\Theta}, \dot{\Theta}\rangle$ is bilinear. If we differentiate with automatic differentiation this mapping with respect to $\dot{\Theta}$, we retrieve $\nabla^2 \mathcal{J}(\Theta)\dot{\Theta}$.
- Because $X(\Theta)$ is fixed, the aforementioned mapping is defined by a single forward recurrence. Hence only one additional backward recurrence should be sufficient to compute $\nabla^2 \mathcal{J}(\Theta)\dot{\Theta}$.

In order to make explicit this backward recurrence, we need to introduce two vectors $A_s \in \mathcal{H}_s$ and $B_s \in \mathcal{G}_s$ that are defined by the implicit equation:

$$\langle A_s, a\rangle_{\mathcal{H}_s} + \langle B_s, b\rangle_{\mathcal{G}_s} = \langle \nabla^2 \mathcal{F}_s(\dot{x}_s, \dot{\theta}_s)\otimes(a,b), \hat{x}_{s+1}\rangle_{\mathcal{H}_{s+1}} \quad \forall (a,b) \in \mathcal{H}_s \times \mathcal{G}_s.$$

The existence and uniqueness of (A_s, B_s) is just Riesz theorem applied to the linear form on $\mathcal{H}_s \times \mathcal{G}_s$:

$$(a,b) \mapsto \langle \nabla^2 \mathcal{F}_s(\dot{x}_s, \dot{\theta}_s)\otimes(a,b), \hat{x}_{s+1}\rangle_{\mathcal{H}_{s+1}}.$$

Construct $\tilde{X} = (\tilde{x}_s)_s$ and $\tilde{\Theta} = (\tilde{\theta}_s)_s$ by a backward recurrence using

$$\begin{cases}\tilde{x}_s = (\partial_x \mathcal{F})^\star \tilde{x}_{s+1} + A_s \quad \text{with } \tilde{x}_{n+1} = 0 \\ \tilde{\theta}_s = (\partial_\theta \mathcal{F})^\star \tilde{x}_{s+1} + B_s.\end{cases} \tag{23}$$

Then we have

$$\nabla^2 \mathcal{J}(\Theta)\dot{\Theta} = \tilde{\Theta} \tag{24}$$

In order to prove (24), we show that for any other direction $\dot{\Theta}'$, we have

$$\langle \nabla^2 \mathcal{J}(\Theta)\dot{\Theta}, \dot{\Theta}'\rangle = \langle \tilde{\Theta}, \dot{\Theta}'\rangle$$

First consider $\dot{X}'$ the tangent associated with direction $\dot{\Theta}'$. We have by bilinearity of $\nabla^2 \mathcal{F}_s$ and by Algorithm 2 that

$$\langle \nabla^2 \mathcal{J}(\Theta)\dot{\Theta}, \dot{\Theta}'\rangle = \sum_s \langle \nabla^2 \mathcal{F}_s(\dot{x}_s, \dot{\theta}_s)\otimes(\dot{x}'_s, \dot{\theta}'_s), \hat{x}_{s+1}\rangle_{\mathcal{H}_{s+1}} = \sum_s \langle A_s, \dot{x}'_s\rangle + \langle B_s, \dot{\theta}'_s\rangle \tag{25}$$

By definition of $\tilde{X}$ and $\tilde{\Theta}$ in (23) and by formula (17) for the tangent $\dot{X}'$, the following equality holds:

$$\begin{aligned}&\langle \tilde{x}_s, \dot{x}'_s \rangle + \langle \tilde{\theta}_s, \dot{\theta}'_s \rangle - \langle A_s, \dot{x}'_s \rangle - \langle B_s, \dot{\theta}'_s \rangle \\ &\quad = \langle (\partial_x \mathcal{F})^\star \tilde{x}_{s+1}, \dot{x}'_s \rangle + \langle (\partial_\theta \mathcal{F})^\star \tilde{x}_{s+1}, \dot{\theta}'_s \rangle = \langle \tilde{x}_{s+1}, \dot{x}'_{s+1} \rangle\end{aligned}$$

Summing up the above equation for every s, using $\tilde{x}_{n+1} = 0$, $\dot{x}'_0 = 0$ and (25) yields (24).

A.3 Proof of Theorem 1

Recall that $(1C, 1M)$ is the complexity of a gradient computation, we show how to change the overall cost of computing the curvature from $(1.5C, 2M)$ to $(2C, 1M)$ by a divide-and-conquer algorithm. In order to simplify the analysis, several simplifications are made.

- There are three kind of passes, the forward pass in (16) that computes X, the backward pass in (18) that computes $\hat{X}$ and $\hat{\Theta}$ and the tangent-curvature pass described in Algorithm 2 that computes the curvature. We suppose that each of these passes have roughly the same computational cost $C/2$. This assumption is subject to discussion. In one hand the backward and tangent passes require each twice as much matrix multiplication as the forward pass. On the other hand, soft activation functions are harder to compute in the forward pass.
- We assume that storing X or $\hat{X}$ has the same memory footprint $1M$. Notably, we suppose that the cost of storing the parameters Θ or the gradient $\hat{\Theta}$ is negligeable with respect to the storage of the data through the network. This assumption can only be made for optimization with large enough batches $\mathcal{B}_k$.
- We suppose that we can divide the neural network in two pieces that each costs half the memory and half the computational time. This means that we are able to find L, such that the storage of $(x_s)_{s \leq L}$ and the storage of $(x_s)_{s \geq L}$ have same memory footprint $M/2$. Moreover we suppose that performing a pass for $s \geq L$ or for $s \leq L$ costs $C/2$ computational time. This assumption is reasonable and simplifies the analysis but it is of course possible to exhibit pathological networks that won't comply with this assumption.
- We suppose that the only cost in data transfer comes from the initialization of the parameters Θ, the initial data x_0 and the direction of descent $\dot{\Theta}$. Note that the computation of $\dot{\Theta}$ requires the computation of the gradient $\hat{\Theta}$.

We now describe how to compute the curvature with $(2C, 1M)$ and no extra data transfer. We display the current memory load and the elapsed computational time at the end of each phase. A visual illustration of this algorithm is proposed in Figure 5.

0. Transfer the data x_0 and Θ.
1. Compute $X = (x_s)_s$ and store it. For $s \geq L$, compute the backward via (14) without storing it. Cost is $(\frac{3}{4}C, 1M)$
2. Flush from memory $(x_s)_{s \geq L}$. Cost is $(\frac{3}{4}C, \frac{1}{2}M)$
3. For $s \leq L$, compute the backward via (14) and store it. Cost is $(1C, 1M)$
4. Choose the descent direction and transfer the data $\dot{\Theta}$. Compute the tangent via (17) for $s \geq L$. Cost is $(\frac{5}{4}C, M)$
5. Flush from memory $(\hat{x}_s)_s$ and $(x_s)_{s<L}$. Cost is $(\frac{5}{4}C, 0M)$
6. For $s \geq L$, compute the forward, the backward and store them. Compute the tangent for $s \geq L$. Cost is $(2C, 1M)$

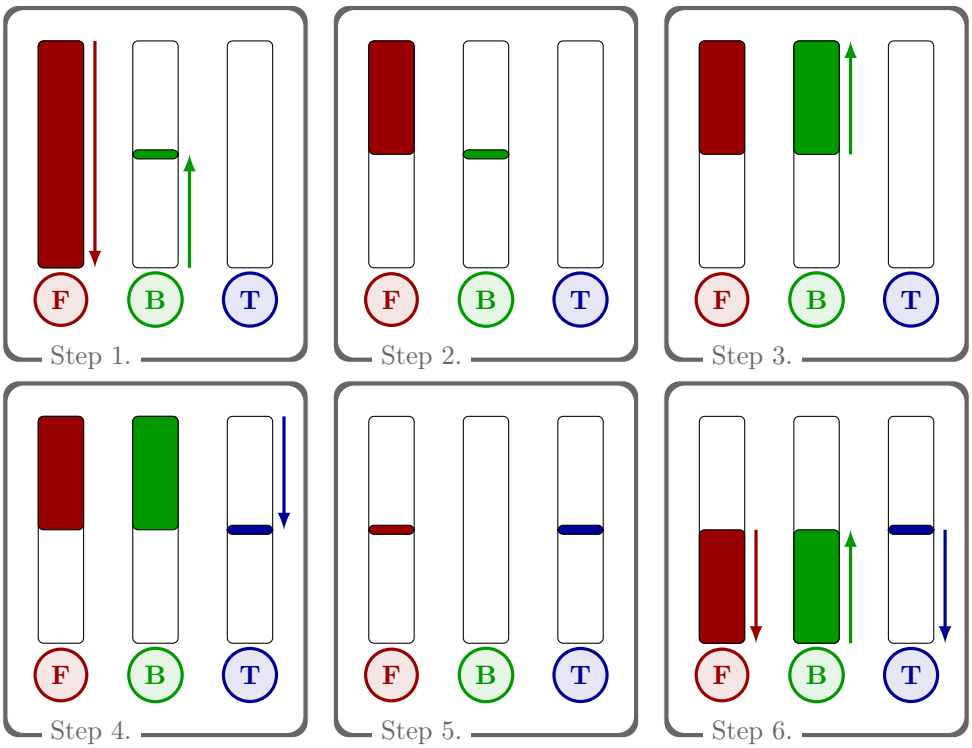

Figure 5: Illustration of the divide-and-conquer algorithm of Section A.3 that changes the cost of computating the curvature from $(1.5C, 2M)$ to $(2C, 1M)$. The rectangles above the letters **F, B, T** represent the three different passes (in order: forward, backward and tangent). The memory usage is represented by color-filling in the rectangles, the computations are represented by arrows on the right of the passes. In total, the filled area never exceeds 1 rectangle, hence memory usage is $1M$. The total length of the arrows is 4 times the length of a rectangle, this represents 4 passes. The computational time is then twice the computational time of the backward algorithm.

A.4 Structure of the layers

In this section, we explain how to compute the curvature for some of the standard layers used in DNNs. First, we make clear the different kind of layers we use:

- **Loss layers** are parameter-free layers from $\mathcal{H}_n$ to $\mathbb{R}$, they are denoted by $\mathcal{L}$

$$\mathcal{F}_n(x, \theta) = \mathcal{L}(x)$$

- **Smooth activation layers** do not have parameters and are such that $\mathcal{H}_{s+1} = \mathcal{H}_s$ and are defined coordinate-wise through a smooth function $\Phi_s : \mathbb{R} \to \mathbb{R}$ with

$$\mathcal{F}_s(x, \theta)[i] = \Phi_s(x[i]) \quad \forall i.$$

- **Linear layers or convolutional layers**. The set of parameters are the weights (or kernel) denoted θ. We suppose that these layers have no bias. They are abstractly defined as

$$\mathcal{F}_s(x, \theta)[i] = \sum_{k,j} \theta[k]x[j]\mathbb{1}_{ijk}$$

  where i (resp j, k) denotes the sets of indices of the outputs (resp. the input, the weights). The function $(i, j, k) \mapsto \mathbb{1}_{ijk}$ represents the assignment of the multi-index (k, j) to i. This affectation is either equal to 1 or 0, that is $(\mathbb{1}_{ijk})^2 = \mathbb{1}_{ijk}$.

- **Bias layers** are layers where $\mathcal{H}_s = \mathcal{H}_{s+1}$ and are defined by

$$\mathcal{F}_s(x, \theta)[i] = x_s[i] + \sum_k \mathbb{1}_{ik}\theta[k].$$

  They are often concatenated with linear or convolutional layers. There is no restriction to split a biased linear layer into the composition of a linear layer and a bias layer.

- **Batch norm-layers.** We split a batch-norm layer into the composition of four different layers, the centering layer, the normalizing layer, a linear layer with diagonal weight matrix and a bias layer. For each output index i, the centering and normalizing layers are defined by an expectation over the batch and some input indices. This expectation is denoted as $\mathbb{E}_i$. The centering layer can be written as

$$\mathcal{F}_s(x, \theta)[i] = x_s[i] - \mathbb{E}_i(x_s).$$

  The normalizing layer is defined as

$$\mathcal{F}_s(x, \theta)[i] = \frac{x[i]}{\sqrt{\mathbb{E}_i(x^2) + \varepsilon}}.$$

For the different layers, we give the formula for the different recurrences in Table 1. We begin with the classic backward computations, they are mainly given here to settle the notations.

B Description of the numerical experiments

All the experiments were conducted and timed using Python 3.8.11 and PyTorch 1.9 on an Intel(R) Xeon(R) W-2275 CPU @ 3.30GHz with an NVIDIA Quadro RTX 5000 GPU. We also used the Jean-Zay HPC facility for additional runs.

The models are trained with a batch size of 256 so that one epoch corresponds to 235 iterations for MNIST and 196 for CIFAR. The number of epochs is set to 200 for the MNIST classification and 500 for the others. Table 2 summarizes the characteristics of the datasets used.

Concerning the tuning of the standard methods, the step size and its decay factor were searched on a grid for the SGD and RMSProp methods. The learning rate is constant per epoch and its value at the n^{th} epoch is given by

$$\tau_n = \tau_0 d^n.$$

Name	$x_{s+1}[i]$	$\hat{x}_s[j]$	$\hat{\theta}_s[k]$
Activation	$\Phi(x_s[i])$	$\Phi'(x_s[j])\hat{x}_{s+1}[j]$	N.A.
Linear	$\sum_{k,j} \theta[k]x_s[j]\mathbb{1}_{ijk}$	$\sum_{k,i} \theta[k]\hat{x}_{s+1}[i]\mathbb{1}_{ijk}$	$\sum_{j,i} \hat{x}_{s+1}[j]x_s[i]\mathbb{1}_{ijk}$
Bias	$x_s[i] + \sum_k \mathbb{1}_{ik}\theta[k]$	$\hat{x}_{s+1}[j]$	$\sum_i \mathbb{1}_{ik}\hat{x}_{s+1}[i]$
Centering	$x_s[i] - \mathbb{E}_i(x_s)$	$\hat{x}_{s+1}[j] - \mathbb{E}_j(\hat{x}_{s+1})$	N.A.
Normalizing	$\begin{cases}\gamma = (\mathbb{E}_i(x_s^2) + \varepsilon)^{-1/2} \\ x_{s+1}[i] = \gamma x_s[i]\end{cases}$	$\gamma\hat{x}_{s+1}[j] - x_s\mathbb{E}_j[\gamma^3 x_s\hat{x}_{s+1}]$	N.A.

Name	$\dot{x}_{s+1}[i]$	$r_s = \frac{1}{2}\langle\nabla^2\mathcal{F}_s(\dot{x}_s,\dot{\theta}_s)\otimes(\dot{x}_s,\dot{\theta}_s),\hat{x}_{s+1}\rangle_{\mathcal{H}_{s+1}}$
Activation	$\Phi'(x_s[i])\dot{x}_s[i]$	$\frac{1}{2}\sum_i \Phi''(x_s[i])\dot{x}_s^2[i]\hat{x}_{s+1}[i]$
Linear	$\sum_{k,j}\left(\theta[k]\dot{x}_s[j] + \dot{\theta}[k]x_s[j]\right)\mathbb{1}_{ijk}$	$\sum_{k,j,i}\dot{\theta}[k]\dot{x}_s[i]\hat{x}_{s+1}[j]\mathbb{1}_{ijk}$
Bias	$\dot{x}_s[i] + \sum_k \mathbb{1}_{ik}\dot{\theta}[k]$	0
Centering	$\dot{x}_s[i] - \mathbb{E}_i(\dot{x}_s)$	0
Normalizing	$\begin{cases}\dot{\gamma} = -\mathbb{E}_i[\dot{x}_s x_s]\gamma^3 \\ \dot{x}_{s+1}[i] = \gamma\dot{x}_s[i] + \dot{\gamma}x_s[i]\end{cases}$	$\begin{cases}\ddot{\gamma} = -\mathbb{E}_i(\dot{x}_s^2)\gamma^3 + 3\mathbb{E}_i(\dot{x}_s x_s)\gamma^5 \\ r_s = \sum_i \frac{1}{2}\left(\dot{\gamma}\dot{x}_s[i] + \ddot{\gamma}x_s[i]\right)\hat{x}_{s+1}[i]\end{cases}$

Table 1: Quantities needed in the forward, backward and second order passes for standard layers.

Dataset	MNIST	CIFAR10	CIFAR100
License	CC BY-SA 3.0	MIT License	Unknown
Size of the training set	60000	50000	50000
Size of the testing set	10000	10000	10000
Number of channels	1	3	3
Size of the images	28×28	32×32	32×32
Number of classes	10	10	100

Table 2: Summary of the datasets used.

We searched amongst the values $\tau_0 \in \{1\times10^n, 5\times10^n\}_{-5\leq n\leq 1}$ for the step size and $d \in \{0.97, 0.98, 0.99, 1\}$ for the step decay on MNIST classification and $d \in \{0.99, 0.995, 1\}$ for the others. After 20% of the total number of epochs, the couple (τ_0, d) that achieves the best training loss decrease is chosen.

For the CIFAR experiments we used data augmentation with a random crop and an horizontal flip. In the CIFAR100 training we added a random rotation of at most $\pm 15°$.

For reproductibility, the values used in the experiments are summarized in Table 3. Unless explicitely stated, these are the default values used in the experiments of this work. The computing time per epoch is reported in Table 3 for each method. The codes of RED are not optimized, especially for the convolution layers where the backward with respect to the parameters is implemented by an additional run of the forward. This explains why RED is twice slower than the standard methods on the CIFAR classifiers which make intensive use of convolution layers. The total computing time to perform all the experiments presented in this work is approximatively 700 hours.

C Additional numerical experiments

C.1 Dealing with momentum

In the core of the paper, only stochastic optimizers without momentum are presented. In this section, we discuss the extension of our algorithm to momentum based update directions, notably momentum with RMSProp preconditioning which is the celebrated Adam algorithm.

Incorporating momentum consists in replacing the gradient by an exponential moving average of the past iterates of the gradients with a parameter $\beta_1 \in [0, 1[$. In our setting, it amounts to replacing line 9 of Algorithm 3 by lines 4 and 5 of Algorithm 4.

Momentum was introduced by Polyak [32] in the convex non-stochastic setting. It can be interpreted as an adaptation of a convex method to a non-convex stochastic problem. We coin this explanation as the *heavy-ball* analysis. Another point of view, which we denote as *variance reduction*,

Type of problem	MNIST classification	CIFAR10 classification	CIFAR100 classification	MNIST autoencoder
Type of network	LeNet Dense	VGG11 Convolutional	VGG19 Convolutional	Dense
Activation functions	Tanh	SoftPlus $\beta = 5$	SoftPlus $\beta = 5$	ELU
L^2 regularization	$\lambda = 10^{-7}$	$\lambda = 10^{-7}$	$\lambda = 10^{-7}$	$\lambda = 10^{-7}$
Loss function	Cross entropy	Cross entropy	Cross entropy	MSE
Number of epoch	200	500	500	500
Batch size	256	256	256	256
Number of epoch for tuning	40	100	100	100
Iteration per epoch	196	235	235	196
Computing time per epoch with the standard SGD / RMSProp	5.3s / 5.4s	16.4s / 16.8s	36.3s / 36.9s	5.1s / 5.3s
Computing time per epoch with auto-SGD / auto-RMSProp	7.6s / 7.7s	30.1s / 30.5s	65s / 65s	5.7s / 5.9s

Table 3: Summary of the experiment parameters.

Algorithm 4 Adding momentum to RED

Initialization $\hat{g}_0 = 0$.
for $k = 1..$ **do**
    $\cdots$
    $\hat{g}_k = \beta_1 \hat{g}_{k-1} + (1 - \beta_1) g_k \quad$ and $\quad \tilde{g}_k = \hat{g}_k / (1 - \beta_1^k)$
    $\dot{\Theta}_k = P_k^{-1} \tilde{g}_k$
    $\cdots$
end for

is that the exponential moving average $\tilde{g}_k$ is a better estimator of $\nabla\mathcal{J}(\Theta_k)$ than g_k. Indeed all the previous batches $(\mathcal{B}_m)_{m\leq k}$ are taken into account in the computation of $\tilde{g}_k$. The downside is that the averaged quantity is $\nabla\mathcal{J}_{\mathcal{B}_m}(\Theta_m)$ and not $\nabla\mathcal{J}_{\mathcal{B}_m}(\Theta_k)$, this introduces a bias in the estimation of $\nabla\mathcal{J}(\Theta_k)$. With this interpretation in mind, the parameter β_1 which drives the capacity of the exponential moving average to forget the previous iterations has to be tuned between the mini-batches gradient variance (high variance leads to high β_1) and the convergence (high values of $\|\Theta_k - \Theta_{k-1}\|$ lead to low choice of β_1). In [19], the authors propose to solve this dilemna by taking decaying values of β_1, although in practice, the parameter β_1 is constant.

Momentum: heavy ball or variance reduction? When momentum is understood as an heavy-ball method, at iteration k there are no reasons for $-\dot{\Theta}_k$ to be a direction of descent. Because our algorithm relies on the assumption that $-\dot{\Theta}_k$ is a direction of descent to choose a step, our analysis falls apart and RED should be used with care. On the other hand, if momentum is a variance reduction technique, the step has to be taken small enough in order not to bias the gradient estimation. With this latter assumption, RED can be applied.

In order to determine if, in our case, momentum acts as an heavy ball method or as a variance reduction technique, we study numerically when the standard Adam and SGD with momentum optimizers yield a direction of descent. In Figure 6, the tests of Section 4.1 (Figure 1) are performed with a momentum $\beta_1 = 0.9$ and the hyperparameters were tuned using the same policy (see Appendix B). We display in the last row of Figure 6 the percentage of direction of descent per epoch with respect to the current batch $\mathcal{B}_k$. If n is the epoch number and $\mathcal{K}_n$ the set of the iterations that are in epoch n, this percentage is given by:

$$q_n = \frac{1}{|\mathcal{K}_n|}\sum_{k\in\mathcal{K}_n} \mathbb{1}_{\langle g_k, \dot{\Theta}_k\rangle \geq 0} \tag{26}$$

We observe that on classification problems, SGD with momentum and more particularly Adam yield directions of update that are not direction of descent for $\mathcal{J}_{\mathcal{B}_k}$. This is even more pronounced on CIFAR10 where this can happen up to 20% of the iterations. Interestingly, this never happens on the autoencoder except for the first iterations. Hence the heavy ball effect is important for the classification problems in consideration.

Step choice The RED algorithm needs a rule to deal with update directions which are not directions of descent. One possibility is to allow negative steps, which we discard since this would annihilate the heavy-ball effect. Another possibility, which we retain, is to take the absolute value of $\tau_k^\star$ in line 11. In a nutshell, compute the step for the opposite direction (which is a direction of descent) and use this step in the current direction. This choice is arbitrary and to properly tackle the momentum case, interpretations using Lyapunov functions should be considered. The choice of such functions is not clear and we defer such an analysis to future work.

In Figure 6 the results of the optimization using RED with momentum are displayed. The parameters for the initial learning rate and its decay factor are the default ones $\ell = 1$ and $\eta = 1/2$. The RED algorithm has difficulties to converge both on the training and testing losses. The steps chosen by RED are several orders of magnitude higher than the ones obtained by manual tuning. On classification problems, RED follows directions of update that are not direction of descent.

Learning rate multiplication The impediment to using RED with momentum is that directions of update are not directions of descent. This can be solved by reducing the initial learning rate ℓ to take smaller steps τ_k so that $\|\Theta_k - \Theta_{k-1}\|$ remains small.

We propose to diminish the initial learning rate by using $\ell = 1 - \beta_1$. This choice may seem arbitrary but it is inspired by the proofs of convergence of [12] that have bounds which scale as $1 - \beta_1$. The experiments of Figure 6 are performed with the same set of parameters except for the initial learning rate which is set to $\ell = 0.1$. This new set of experiments is given in Figure 7. With this smaller learning rate, the algorithm is stable and converges. However, RED outperforms the standard SGD with momentum and Adam only on MNIST. Of importance, on the CIFAR tests, RED always yield direction of descent as seen from the last row of Figure 7. As ℓ was decreased, the exploration is lost and hence the convergence is worse, explaining these poor convergence results.

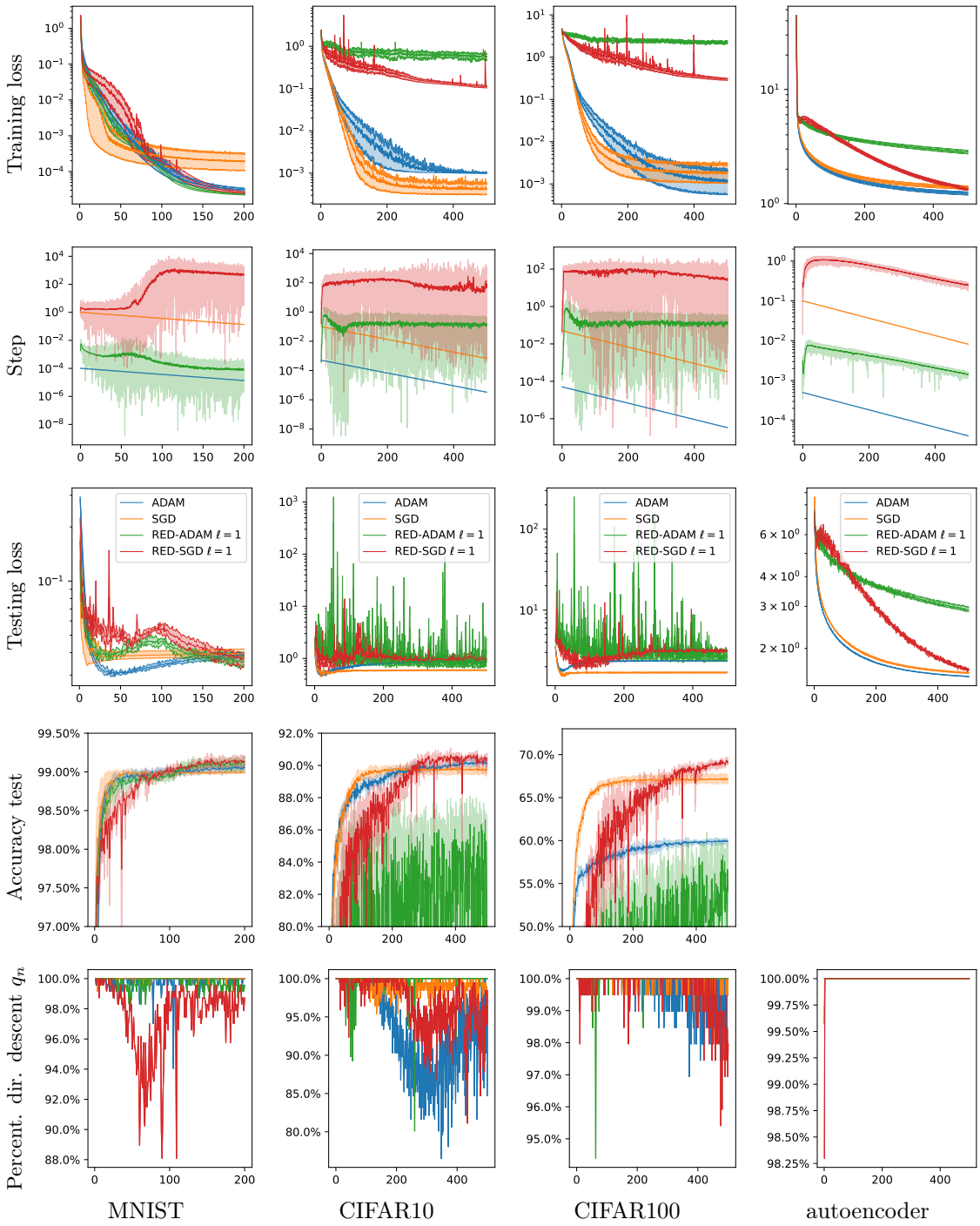

Figure 6: Tests with momentum ($\beta_1 = 0.9$) and $\ell = 1$ for RED. Manually-tuned algorithms (orange for SGD, blue for Adam) and their RED version (red for SGD, green for Adam) are given. Momentum does not necessarily yield directions of descent (see last row), this turns RED into an unstable algorithm.

Conclusion When using momentum, multiplying the steps found by RED by $1 - \beta_1$ makes the experiments fit in the framework the algorithm was proposed for. As a consequence, this causes the loss of the exploration which is critical to speed-up the convergence. The correct way of dealing with momentum would be to identify the Lyapunov function that has to be minimized, which is left for future work.

C.2 Effect of the L^2 regularization

An L^2 regularization is introduced in our algorithm to counteract the effet of a vanishing Hessian in the direction of update. This is a theoretical limitation and we study in this section the influence of this regularization on the performance of RED. The same experiments than Section 4.1 are conducted with different values of the regularization $\lambda \in \{10^{-7}, 10^{-4}\}$. The CIFAR100 classifier is excluded from the experiments for computational cost reasons and because it did not give much additional information for the comparison of the methods. The hyperparameters of the standard SGD and RMSProp optimizers are tuned for each value of λ. We report in Figure 8 the different results, including the ones that are shown in Section 4.1. For the MNIST and autoencoder test cases, RED is always better than standard methods. On CIFAR10, the results are more mitigate as RMSProp outperforms RED on the training loss when $\lambda = 10^{-4}$ but from the test accuracy, our method still gives better generalization. On all test cases, we observe that a value of regularization close to zero ($\lambda = 10^{-7}$) gives good convergence results. In the considered tests, the need of a regularization seems to be more of a theoretical limitation than a practical one.

C.3 Impact of the network structure

This section is dedicated to the illustration of cases where the structure of the network highly impacts the performance of the RED method. We change the structure of the networks by changing their activation functions. The activation functions of the VGG networks in the CIFAR classifiers are replaced by ELU functions, and by SoftPlus in the autoencoder. In Figure 9 the tests of Section 4.1 are presented with the manually-tuned and RED methods on 3 of the experiments. These 3 experiments use a regularization $\lambda = 10^{-7}$ and we also give the results for $\lambda = 10^{-4}$ on the autoencoder.

The conclusions of Section 4.1 are still valid but less pronounced. The convergence of RED is much worse on the training loss for CIFAR100 while the test accuracy remains much better than the standard methods for classification. On the autoencoder, auto-SGD is not very fast but auto-RMSProp is excellent. An explanation of the poor behavior on the autoencoder for auto-SGD could be the lack of batch normalization.

C.4 Influence of the step size and of the decay factor

The influence of the initial learning rate ℓ and its decay factor η is studied in Section 4.2. We presented the tests only for RMSProp preconditioning on CIFAR10. In Figure 10, we report additional experiments on the CIFAR10 classifier and on the MNIST autoencoder with the same set of values for ℓ and η that are used in Figure 2.

The same conclusions as in Section 4.2 can me drawn. On all tests, the values that achieve one of the best decay of the training loss are $\ell = 1$ and $\eta = 1/2$. On CIFAR10 with auto-SGD we observe that the values $(\ell, \eta) = (1, 1)$ give slightly better results than $(1, 1/2)$ but with the auto-RMSProp optimizer, this first set of values results in instabilities. Concerning the autoencoder, surprisingly the values $\ell = 2$ and $\eta = 1/4$ give the best convergence after 500 epochs. We believe it is because the autoencoder is more stable than the CIFAR10 classifier and that the good convergence of the automatic methods on the autoencoder with $\ell = 2$ is a fluke.

C.5 Comparison with BB and Robbins-Monro

In this section we compare our algorithm with the closest existing approach [8], named *step-tuned*, where the authors approximate the curvature with a BB method. We also compare it with a Robbins-Monro decay rule of the learning rate. We did not compare with the BB-method of [46] as this method requires the computation of the gradient over the whole dataset at each epoch.

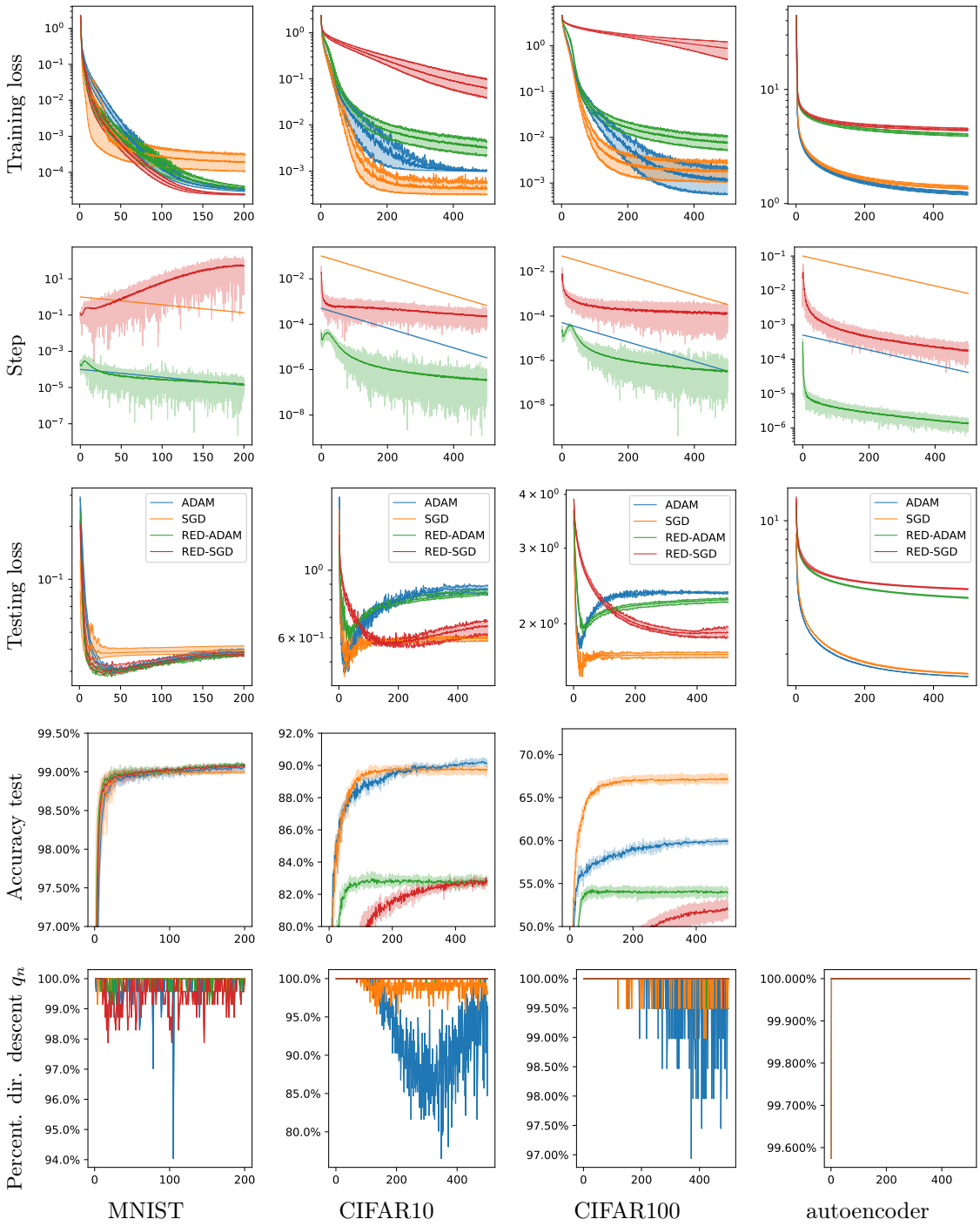

Figure 7: Tests with momentum ($\beta_1 = 0.9$) and learning rate stabilization $\ell = 1 - \beta_1 = 0.1$ for RED. Manually-tuned algorithms (orange for SGD, blue for Adam) and their RED version (red for SGD, green for Adam) are given. Lower learning rate in RED ensures that momentum yields direction of descent at the expense of loosing the exploration of the set of parameters.

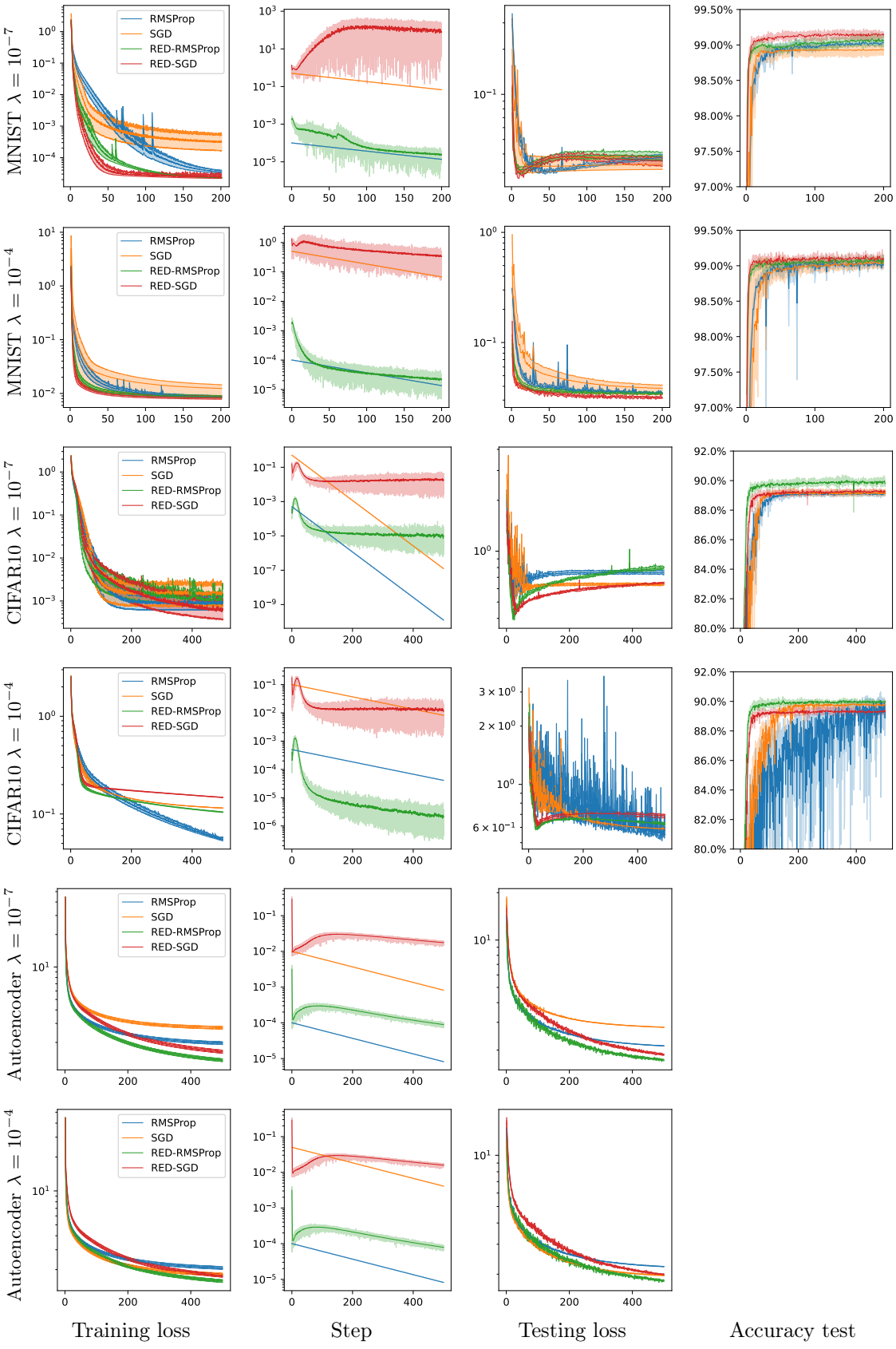

Figure 8: Influence of the L^2 regularization λ. Manually-tuned algorithms (orange for SGD, blue for RMSProp) and their RED version (red for SGD, green for RMSProp) are given. For these tests, the smaller the regularization, the best the convergence of RED.

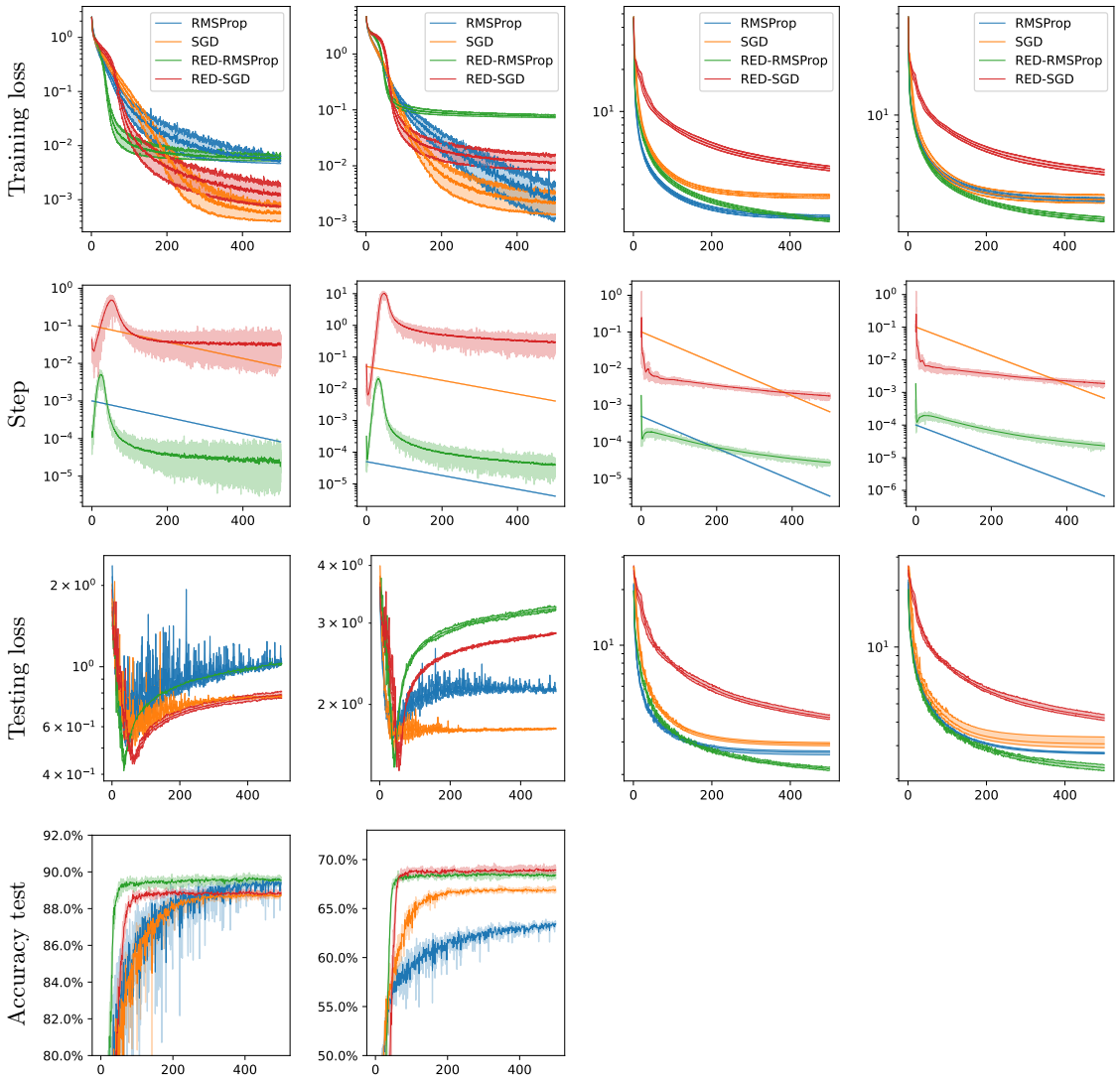

Figure 9: Impact of the activation functions. For the autoencoder we conduct the experiments with two values of the L^2 regularization $\lambda = 10^{-7}$ and $\lambda = 10^{-4}$. Manually-tuned algorithms (orange for SGD, blue for RMSProp) and their RED version (red for SGD, green for RMSProp) are given.

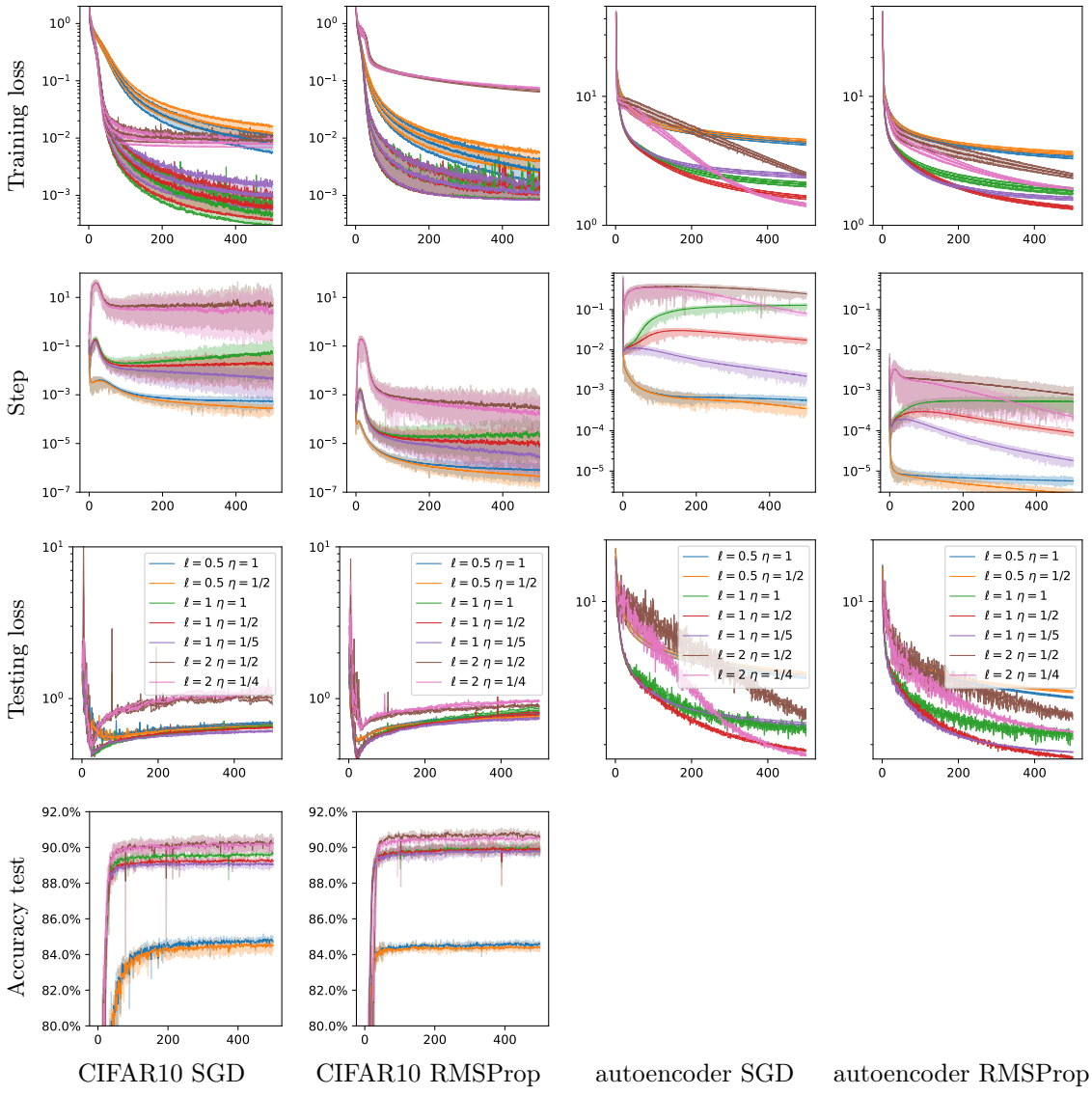

Figure 10: Influence of the step size ℓ and of the decay factor η. Each column gives the different automatic optimizers (SGD and RMSProp) on different test cases (CIFAR10 classifier and MNIST autoencoder). This figure sums up the experiments of Figure 2 with additional tests which lead to the same conclusions.

The step-tuned optimizer has several hyperparameters and we use the default ones except the learning rate as advised in [8]. The initial learning rate of [8] is searched on the same grid than the standard SGD (see Appendix B).

In Figure 11, the results of the optimization on the CIFAR10 classifier and on the autoencoder are given for two values of the L^2 regularization $\lambda \in \{10^{-7}, 10^{-4}\}$. RED algorithm is outperformed by step-tuned only on the training loss of the CIFAR10 classifier but the learning rate of step-tuned has been optimized for the training loss and we cannot expect better performance than step-tuned on this criterion. It has been reported in [8] that step-tuned has poor performance on the autoencoder. RED is significantly faster on this latter experiment. Finally, RED is more stable on every test metrics and has better generalization than step-tuned. Step-tuned [8] requires the optimization of the learning rate and because RED does not need any hyperparameter adjustment, our method is competitive with this existing work. Note also that step-tuned is not available on RMSProp conditionner, when RED handles any kind of preconditionning technique.

In Figure 12, a comparison between RLD and SGD with an exponential decay is given. The RLD algorithm is run with two different decay values: $\eta = 1/2$ is the standard value proposed in the algorithm and $\eta = 1/20$ is given in order to obtain the same decay as the standard SGD at the end of the training process. We observe that on all tests, RED-SGD with $\eta = 1/20$ is outperformed by RED-SGD with $\eta = 1/2$. It seems that the decay with $\eta = 1/20$ is too fast and does not let the algorithm explore the space of parameters.

D Quantile plots

In this section, we display another representation of the step and train loss function of the numerical experiments. Indeed, we choose to perform an exponential moving average of this two quantities in order to smooth the corresponding convergence curves, this might impede with interpretation of the curves. In this section, we display the per-epoch quantiles $(5\%, 25\%, 50\%, 75\%, 95\%)$ of the curves of one run. The quantile display allows assessing the spread of the train loss function and of the step amongst the different batches. The quantiles $(5\%, 50\%, 95\%)$ are represented by lines, the shaded area is the zone between quantile 25% and 75%.

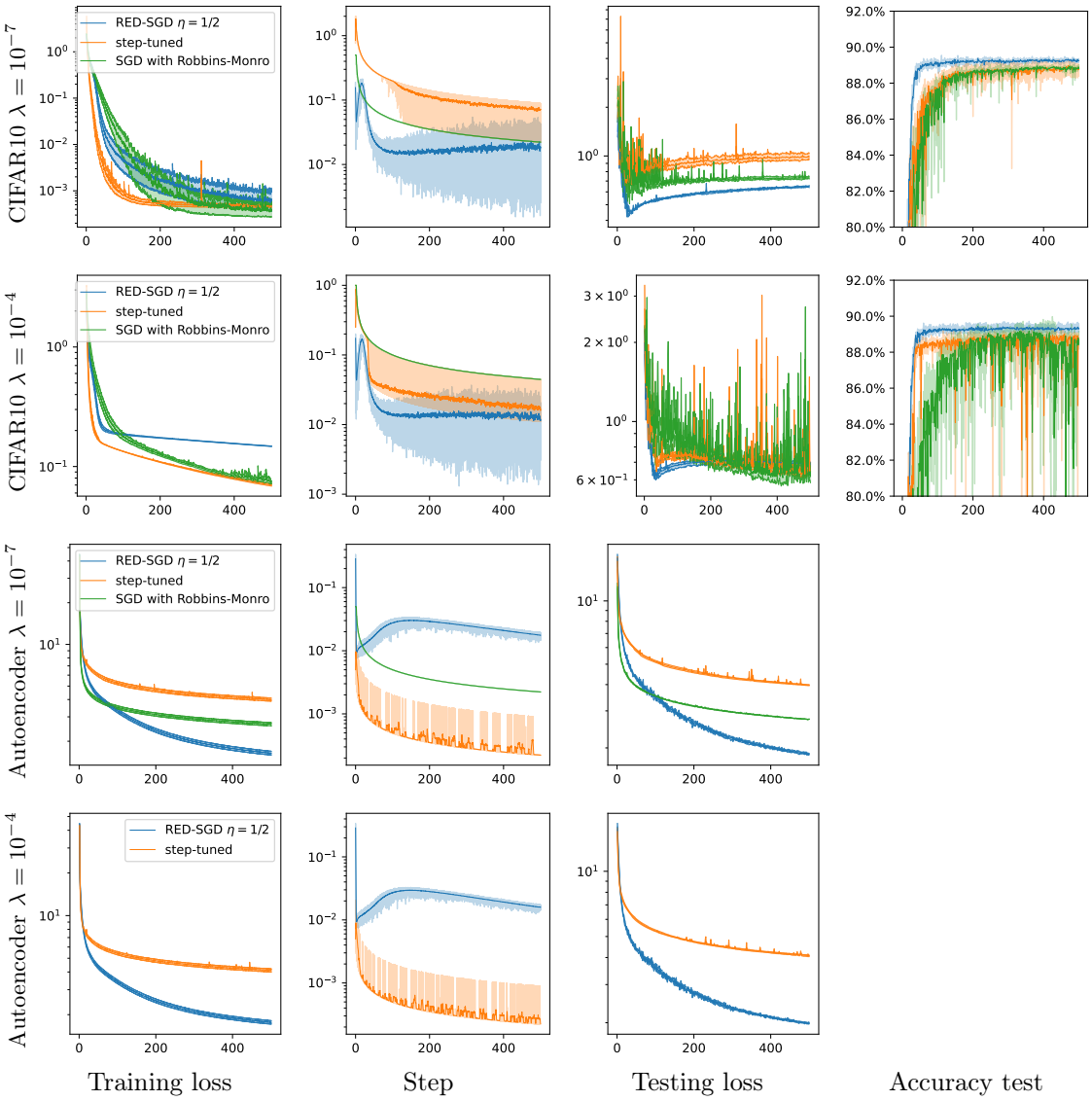

Figure 11: Comparison with step-tuned [8] method. Standard SGD (blue), RED (orange and green) and step-tuned (red) are given. RED is competitive with step-tuned except on the training loss of the CIFAR10 classifier for which step-tuned is optimized.

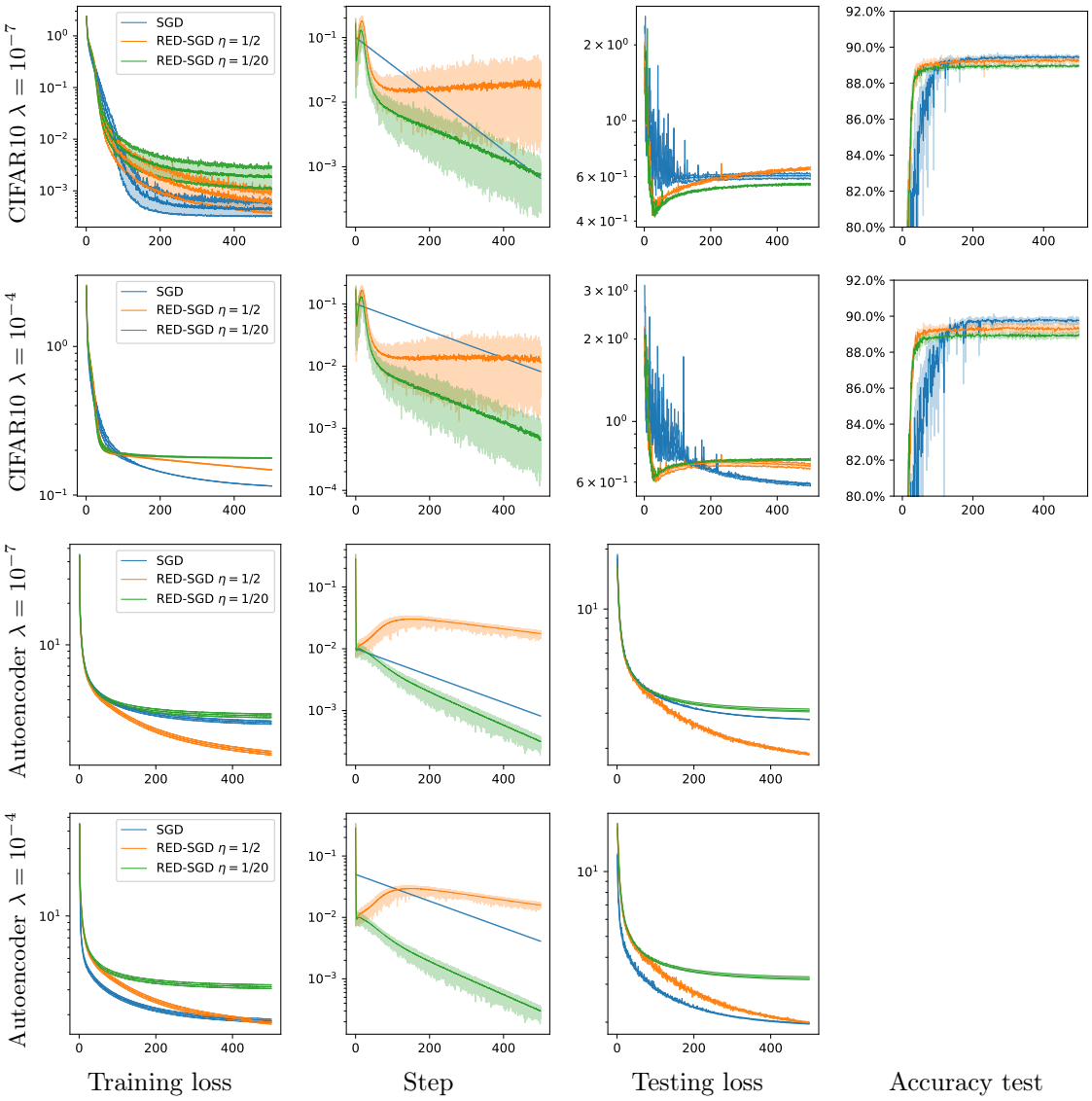

Figure 12: Comparison with SGD and different learning rate decays. Standard SGD (blue), auto-tuned (orange and green) and step-tuned (red) are given. Auto-tuned is competitive with step-tuned except on the training loss of the CIFAR10 classifier for which step-tuned is optimized.

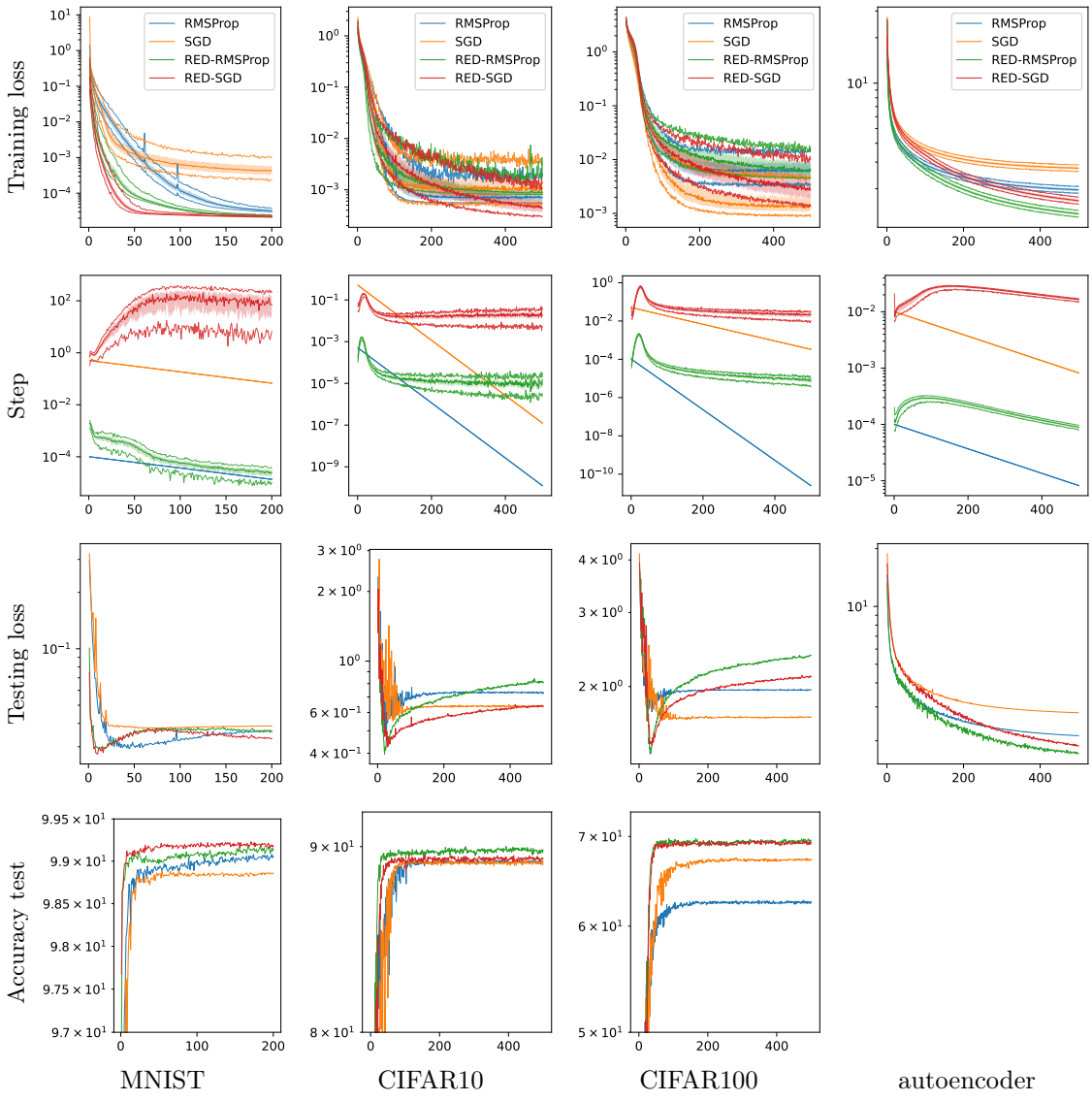

Figure 13: Quantile plot of Figure 1

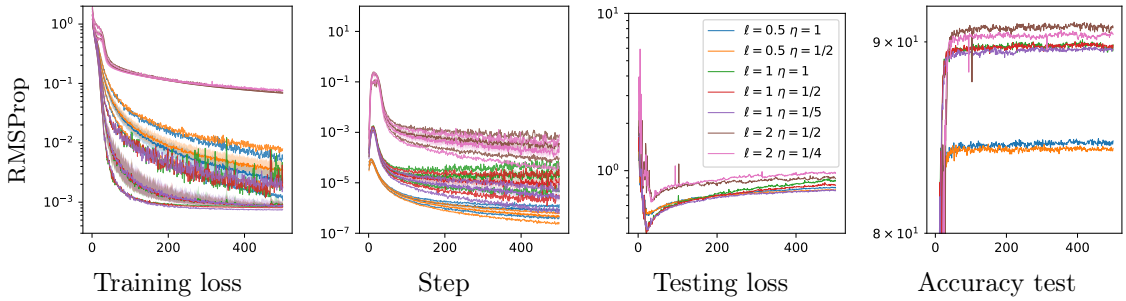

Figure 14: Quantile plot of Figure 2

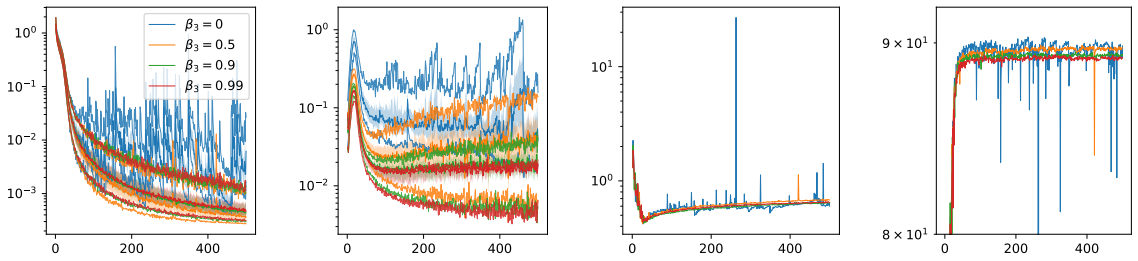

(a) Training loss (b) Step (c) Testing loss (d) Accuracy test

Figure 15: Quantile plot of Figure 4

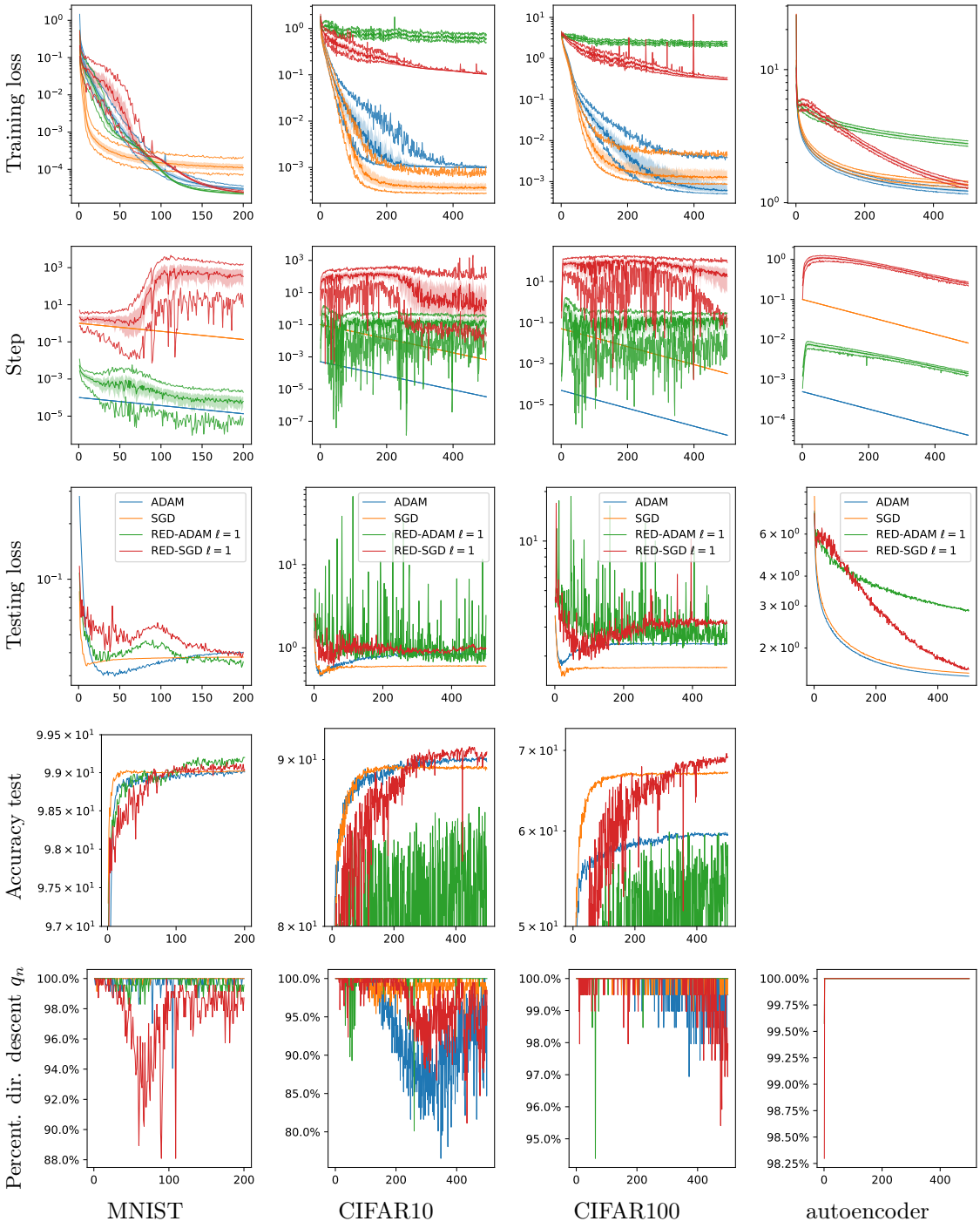

Figure 16: Quantile plot of Figure 6

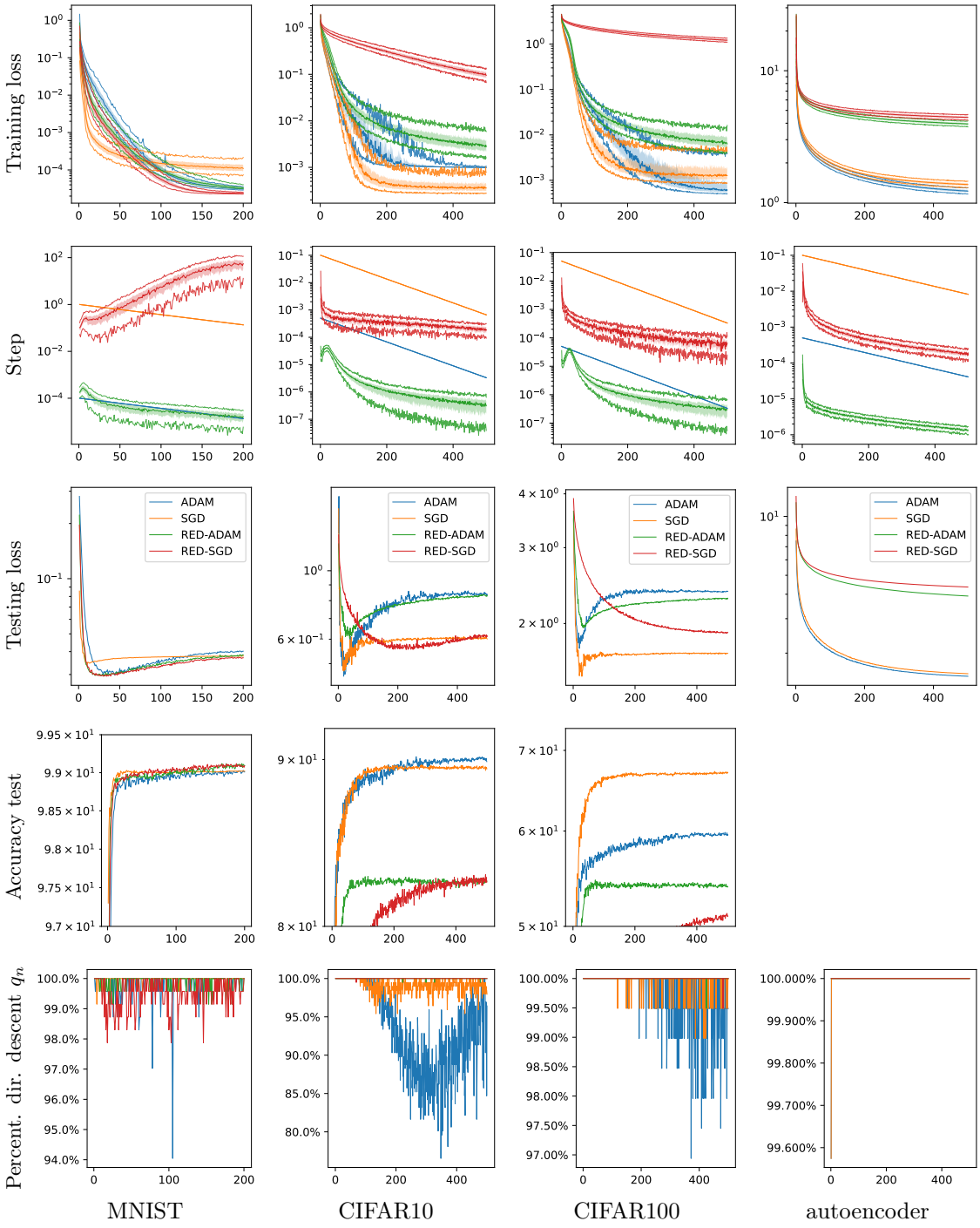

Figure 17: Quantile plot of Figure 7

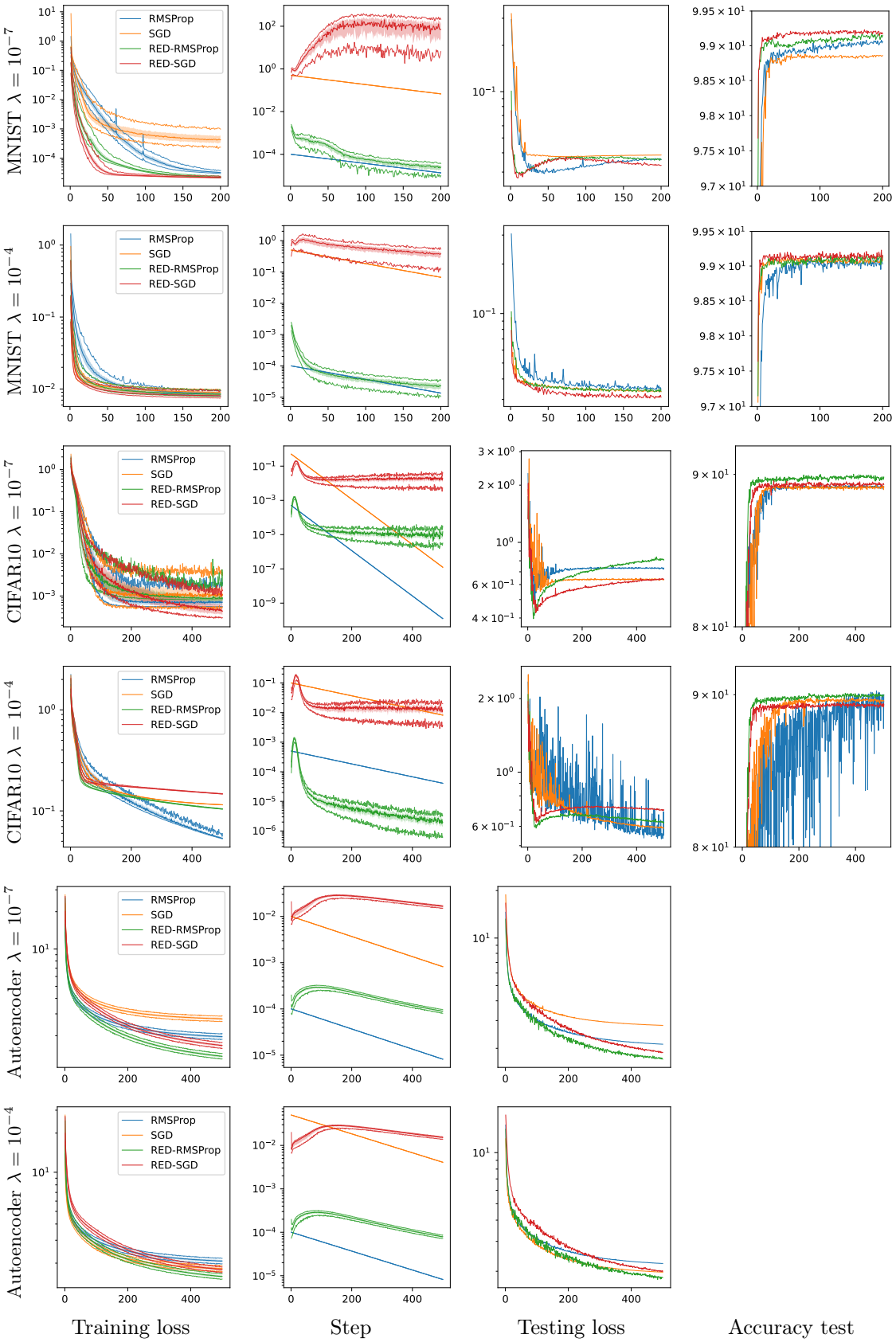

Figure 18: Quantile plot of Figure 8

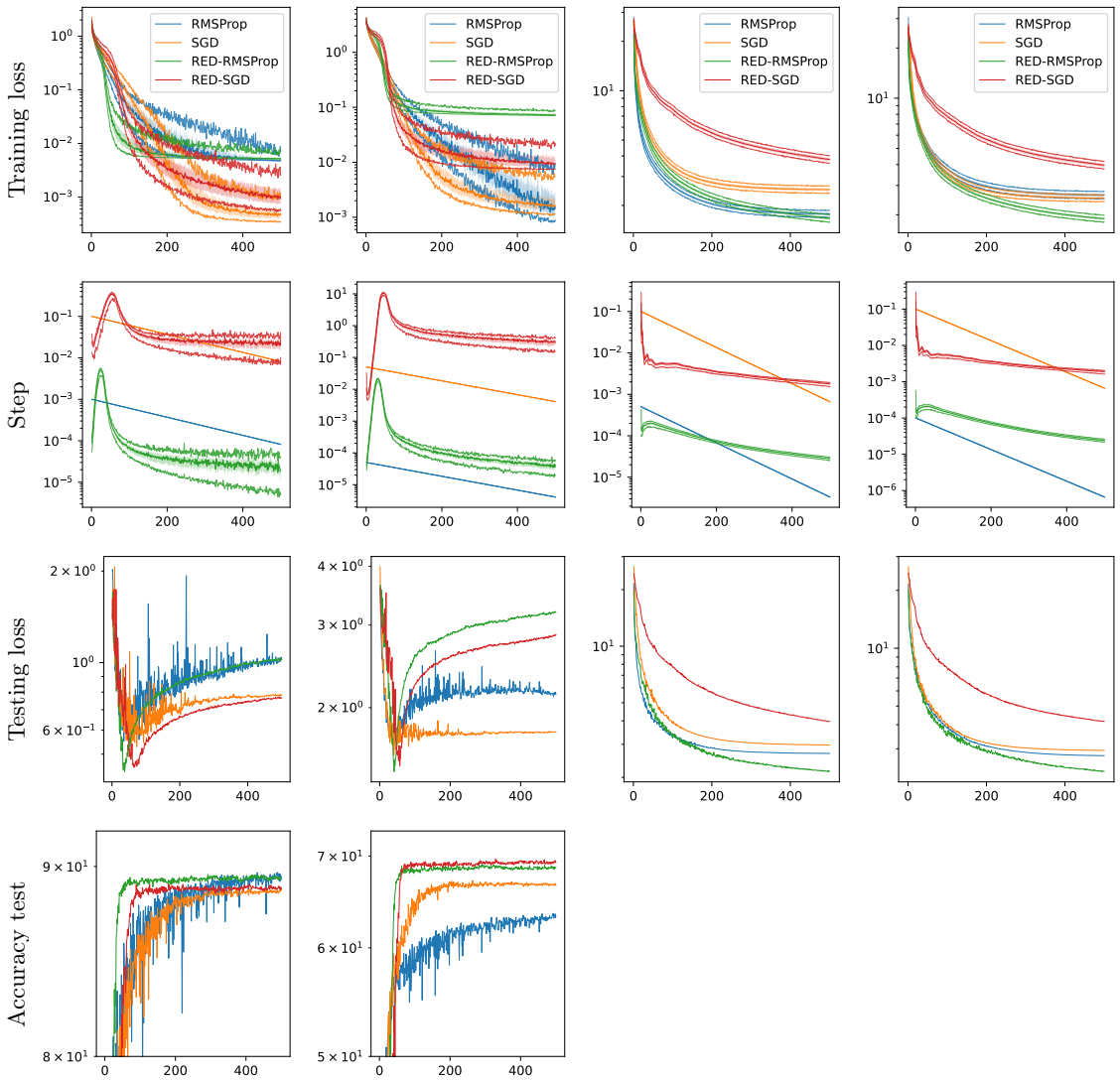

Figure 19: Quantile plot of Figure 9

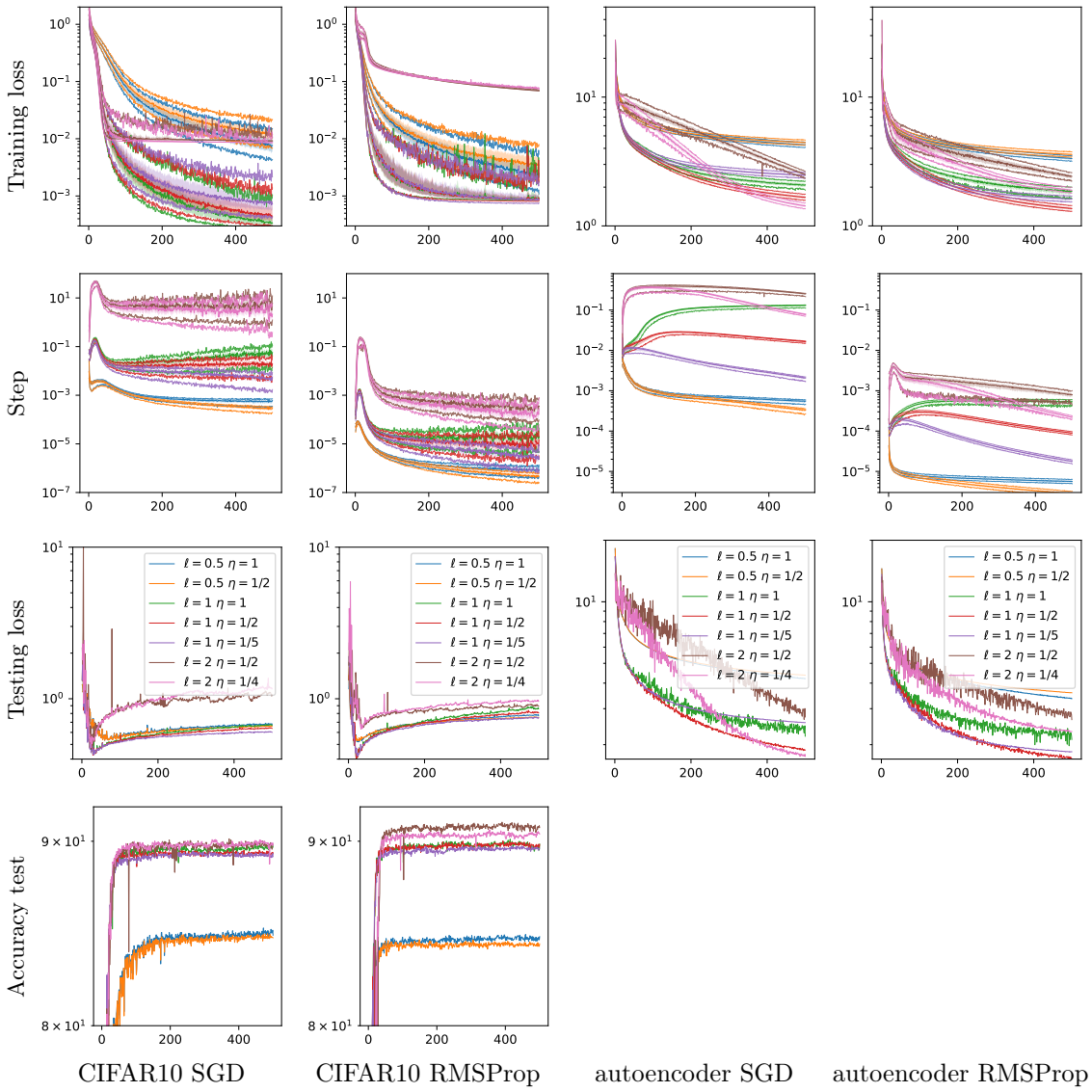

Figure 20: Quantile plot of Figure 10

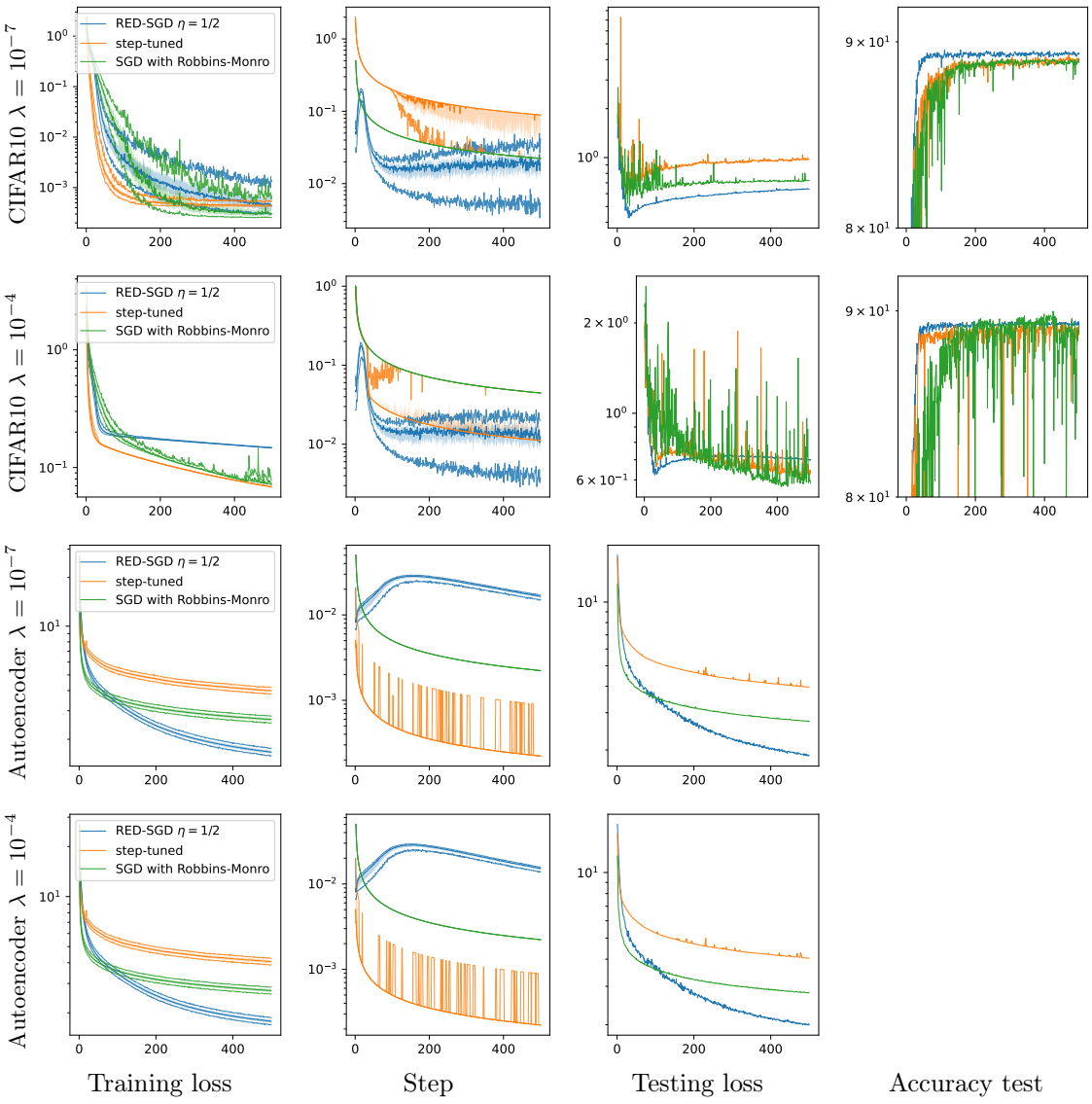

Figure 21: Quantile plot of Figure 11

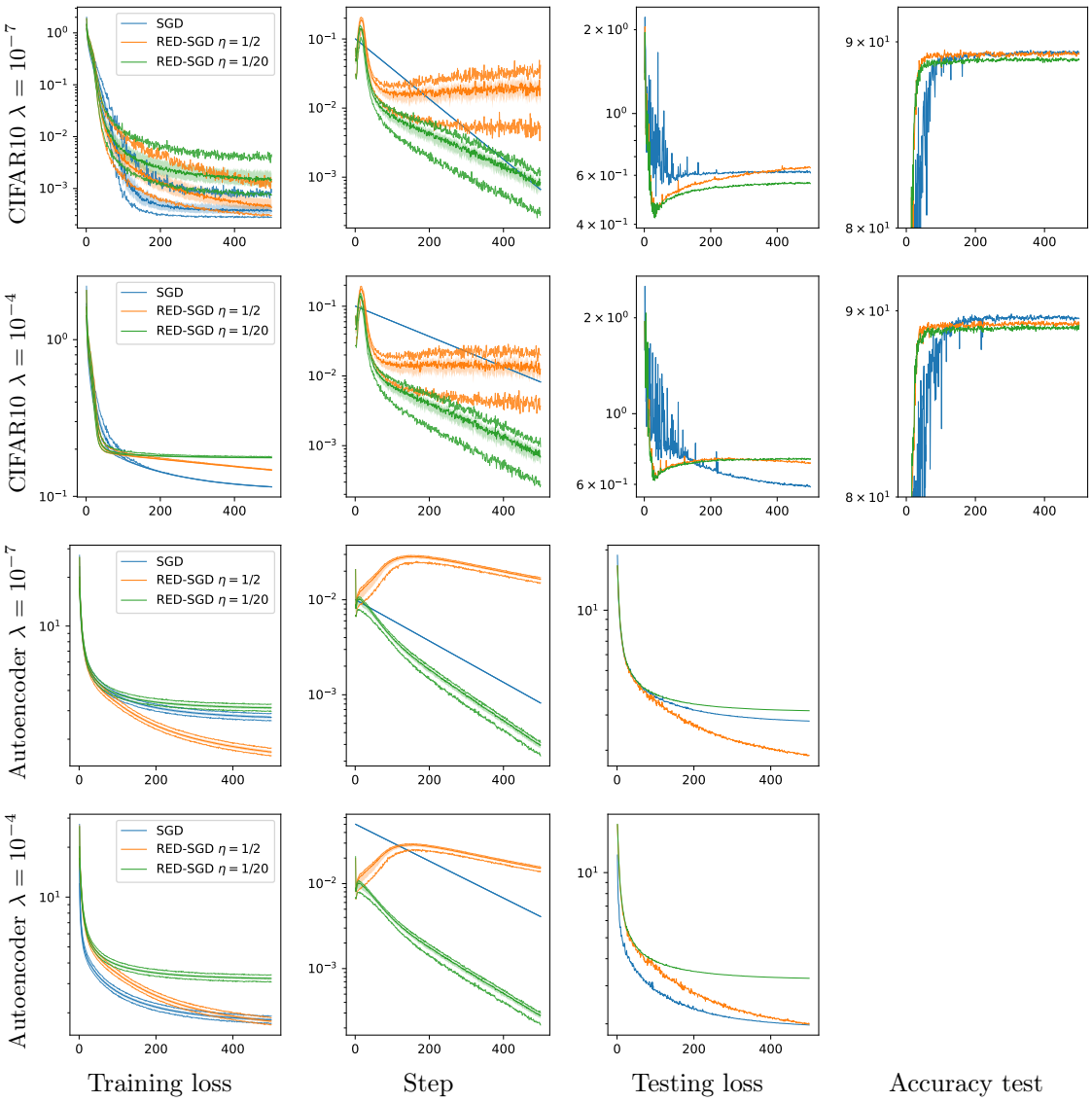

Figure 22: Quantile plot of Figure 12